

ATP DEPENDENT ION TRANSPORT IN BIOMEMBRANES

PhD Thesis

Csilla-Mária Ferencz

Supervisor
Dr. Tibor Páli

Institute of Biophysics
Biological Research Centre
Hungarian Academy of Sciences
Szeged, Hungary

2012

Table of Contents

ACKNOWLEDGEMENTS	iii
PAPERS RELATED TO THE THESIS	iv
LIST OF ABBREVIATIONS	iv
INTRODUCTION.....	1
1. LITERATURE.....	3
1.1. STRUCTURE AND MECHANISM OF VACUOLAR H ⁺ -ATPase	3
1.1.1. Structure and assembly of yeast <i>Saccharomyces cerevisiae</i> vacuolar H ⁺ -ATPase and bacterial F-ATPase	3
1.1.1.1. V ₁ : the catalytic domain.....	4
1.1.1.2. V _o : proton translocation across the membrane	5
1.1.2. Catalysis and ion transport coupled by a rotary mechanism in V-ATPase	6
1.2. STRUCTURE AND MECHANISM OF Na,K-ATPase.....	10
1.2.1. Structure of Na,K-ATPase.....	10
1.2.2. Catalytic mechanism of Na,K-ATPase	11
2. THE AIM OF THE WORK.....	14
3. MATERIALS AND METHODS	15
3.1. CHEMICALS	15
3.2. CULTURE OF YEAST CELLS.....	15
3.3. ISOLATION OF VACUOLES AND PREPARATION OF VACUOLAR MEMBRANE VESICLES	15
3.4. LIGHT MICROSCOPY OF YEAST VACUOLES	16
3.5. FREEZE-FRACTURE ELECTRON MICROSCOPY OF VACUOLAR MEMBRANE VESICLES	16
3.6. VACUOLAR H ⁺ -ATPase ACTIVITY ASSAY	17
3.7. VACUOLAR H ⁺ -ATPase UNDER OSCILLATING ELECTRIC FIELD	18
3.8. Na,K-ATPase ENZYME PREPARATIONS	18
3.9. SAMPLE PREPARATION FOR DIFFERENTIAL SCANNING CALORIMETRY	19
3.10. DIFFERENTIAL SCANNING CALORIMETRY.....	19
4. RESULTS AND DISCUSSION	21
4.1. MORPHOLOGY AND FUNCTION OF YEAST <i>SACCHAROMYCES CEREVISIAE</i> VACUOLES AND VACUOLAR MEMBRANE VESICLES	21
4.2. ROTARY MECHANISM OF VACUOLAR H ⁺ -ATPase UNDER OSCILLATING ELECTRIC FIELD	30
4.3. THE TWO-CHANNEL MODEL	32
4.4. DIFFERENTIAL SCANNING CALORIMETRY OF SHARK Na,K-ATPase CONTAINING MEMBRANES	35
4.5. DIFFERENTIAL SCANNING CALORIMETRY OF PIG KIDNEY Na,K-ATPase CONTAINING MEMBRANES	37
SUMMARY.....	41
REFERENCES	43

Acknowledgements

This dissertation is the result of a research project carried out at the Institute of Biophysics, Biological Research Centre, Hungarian Academy of Sciences.

I especially want to express my sincere appreciation and gratitude to my supervisor Dr. Tibor Páli, for taking me on to do this project in the first place, for his encouragement and guidance during my research and introducing me into the fascinating biophysical world. His ideas and tremendous support had a major influence on this thesis and his well intentioned advice saved me many times from difficulties. He has been a constant presence throughout my PhD and was able to keep me motivated, challenged and productive at all time.

I am greatly indebted to Prof. Pál Ormos, head of the Biological Research Centre and Institute of Biophysics for giving me the opportunity to work at the Institute.

I would like to express many thanks to my colleges Dr. Elfrieda Fodor-Ayaydin and Dr. Zoltán Kóta for their inspiring ideas, advices and for providing me all of their scientific and technical experience.

Special thanks to Dr. András Dér for his help in setting up the measurement with the electric field, to Dr. Ferhan Ayaydin and Dr. Attila Bóta for their help in light and electron microscopy investigations. Their collaboration is greatly acknowledged.

Thanks to Dr. Mikael Esmann and Dr. Natalya U. Fedosova for providing us the Na,K-ATPase samples and for their help in the discussion of differential scanning calorimetry results.

I am grateful to Dr. Balázs Szalontai for carefully reading my thesis and helping me to improve it.

I would like to thank all people who have helped and inspired me during my doctoral study and my friends who made my stay in Szeged enjoyable.

Papers related to the thesis

1. **C. Ferencz**, P. Petrovszki, Z. Kóta, E. Fodor-Ayaydin, L. Haracska, A. Bóta, Z. Varga, A. Dér, D. Marsh, T. Páli
Estimating the Rotation Rate in the Vacuolar Proton-ATPase in Native Yeast Vacuolar Membranes
European Biophysics Journal, (*in press*, DOI 10.1007/s00249-012-0871-z).
2. E. Fodor, NU. Fedosova, **C. Ferencz**, D. Marsh, T. Pali, M. Esmann
Stabilization of Na,K-ATPase by ionic interactions
Biochimica et Biophysica Acta - Biomembranes 1778, 835-843 (2008).

List of Abbreviations

CDTA	Trans-1,2-cyclohexylenedinitrilo-tetraacetic acid
DCCD	N,N-di-cyclohexylcarbodiimide
DSC	Differential scanning calorimetry
DTT	DL-Dithiothreitol
EDTA	Ethylenediaminetetraacetic acid
FCCP	Carbonyl cyanide 4(trifluoromethoxy)phenylhydrazone
MES	2-(N-Morpholino)ethanesulfonic acid hydrate
Na ₂ ATP	Adenosin-5'-triphosphate disodium salt hydrate
NaN ₃	Sodium azide
Na ₃ VO ₄	Sodium orthovanadate
NEM	N-Ethylmaleimide
SDS	Dodecyl sodium sulphate
TM	Transmembrane
TRIS	Tris(hydroxymethyl)aminomethane
V-ATPase	Vacuolar or v-type proton-ATPase

Introduction

ATP is a universal energy currency in all living organisms. It is consumed in the vast number of energy requiring chemical processes in the cell. According to estimation, a human utilizes 40 kg of ATP in normal daily living and 90% of the ATP in the human body is produced by the F-ATPase enzyme. However, F-ATPase is not the only enzyme of its kind. An increasing number of studies is being dedicated to the fascinating family of enzymes consisting of the A-type, F-type, V-type and P-type ATPases. These different types of membrane-associated ATPases have evolved over time to meet specific demands of cells. They all catalyze the reaction of ATP synthesis and/or hydrolysis; they are membrane-bound ion transporters that couple ion movement through a membrane with the synthesis or hydrolysis of the nucleotide. These enzymes are key players in the energy metabolism of the organisms. They are universal energy converters and the smallest known molecular engines, which make them interesting not only for biochemistry and biophysics but also for the fast-developing field of nanotechnology.

The ATPase family may have only four members, but each one plays a fundamental role in biological energy conversion. The F_1F_0 -ATPases couple ATP synthesis to the electrochemical membrane potential in bacteria, mitochondria and chloroplasts, while the vacuolar H^+ -ATPase operates as an ATP driven proton pump in eukaryotic membranes. In different species of archaea and bacteria, the A_1A_0 -ATPase can function as either an ATP synthase or an ion pump. The P-ATPases are ion pumps that are found in bacteria, archaea and eukaryotes. A-, F- and V-ATPases are rotary molecular motors, sharing a fundamentally similar mechanism, in which rotational movement couples the energy conversion process with ion transport. Even though the two types of enzyme protein complexes used in our experiments, namely the V-type H^+ -ATPase and the P-type Na,K-ATPase, have been investigated for decades, numerous questions remain unanswered regarding their structure, function and mechanism.

The P-ATPases are quite distinct from what in the ions they transport, and do not appear to use a rotary motor. The P-ATPase used in our study is the Na,K-ATPase, which is a central player in mammalian cell physiology. The enzyme was isolated from the salt gland of *Squalus acanthias* and from pig kidney. The proteins derived from these two organisms are

almost identical but they function at different temperatures. The goal was to investigate the effect of ionic strength and low concentrations of cations on the thermo stability and thermal unfolding of Na,K-ATPase, using differential scanning calorimetry.

Our research focused on V-type H⁺-ATPase from *Saccharomyces cerevisiae*, to better understand its mechanism, and structure-activity relationship, as it is very important in the acidification of various intracellular compartments, which in turn is important for a variety of cellular functions. Furthermore, V-ATPase is a potential therapeutic target in certain diseases such as osteoporosis, deafness and cancer [1-5].

Several studies provided a better understanding of the functions of V-ATPase. However, insights into the rotary mechanism and structure required the protein to be isolated from its native environment and to be reconstituted into an artificial one, and to be genetically modified rendering attachment of fluorescent actin filaments or nano particles to the rotating part possible (**Figure 1**) [6].

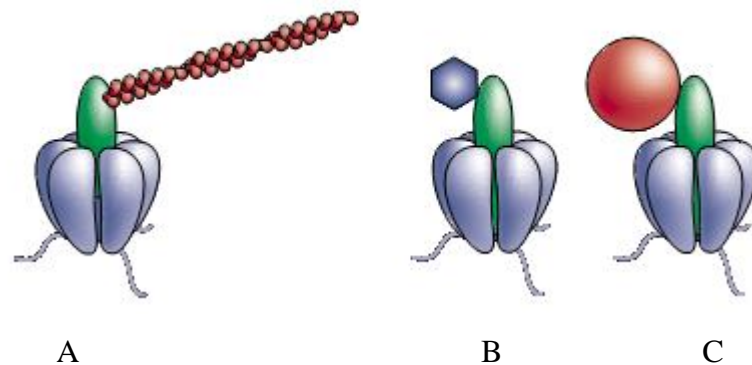


Figure 1: Microprobes to detect the rotation of a nanomotor: A. fluorescently labeled actin filament (1–4 μm); B. single fluorescent dye (~ 2 nm); C. bead (gold (40 nm) or polystyrene (0.5 μm)).

In the present study, we first standardised the conditions of steady state ATPase activity measurements, then worked out a new non-invasive approach to determine the rotation of V-ATPase based on activity measurements in native membranes, under the influence of oscillating electric field and without using any labels or attached particles. In the literature, only a few studies were published to date concerning the effect of oscillating electric field on membrane proteins, but none of them was made on V-ATPase.

1. Literature

1.1. Structure and mechanism of vacuolar H⁺-ATPase

1.1.1. Structure and assembly of yeast *Saccharomyces cerevisiae* vacuolar H⁺-ATPase and bacterial F-ATPase

The structure of the vacuolar type H⁺-translocating ATPase (V-ATPase) has been intensively studied during the past few years. The V-ATPase is a complicated, multicomponent protein complex, evolutionarily related and structurally similar to the F-ATP-synthase (F-ATPase), which is responsible for ATP production in mitochondria, chloroplasts and many eubacteria [7-13]. The structure of both F- and V-ATPases can be divided into two major components: to the water soluble-protein containing extra-membranous, catalytic domains, and to the intra-membranous, F_o and V_o domains, respectively. Each domain contains several subunits. Proposed structures and subunit compositions of the bacterial F-ATPase and the yeast V-ATPase are shown in **Figure 2**.

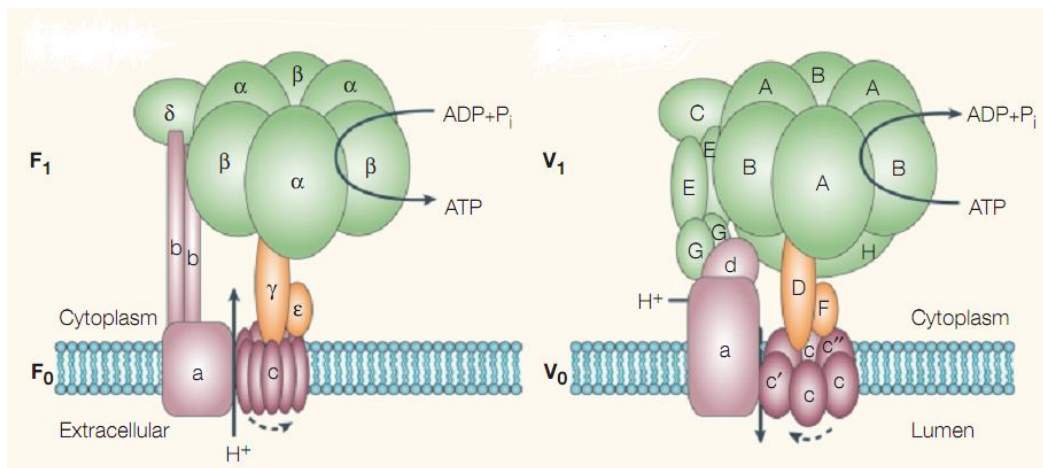


Figure 2: Structure of *Escherichia coli* F-ATPase (left) and yeast *Saccharomyces cerevisiae* V-ATPase (right) [9]. The subunits of the F_o and V_o membrane sectors are shown in pink, and those of the F₁ and V₁ catalytic domains are shown in green and orange. In F-ATPase, the c-, γ - and ϵ - subunits rotate; in V-ATPase, the c- (c, c' and c''), D- and F-subunits.

In V-ATPase, the water-soluble V_1 domain (F_1 domain in F-ATPase) contains the three catalytic site responsible for ATP hydrolysis (synthesis in F-ATPase); the membrane-embedded V_o (F_o) domain is involved in proton transport, which takes place in hydrophilic channels at the interface between the “ c -ring” and subunit a . The key elements for proton transport are the single glutamic acid residues, one on each c -subunit. Specific membrane inhibitors, binding to these acidic residues and blocking the proton transport and ATP hydrolysis [14; 15], demonstrate that the two main functions of the enzyme - catalysis and transport - are coupled. In both enzymes, this coupling is performed by the rotation of the rotor relative to the rest of the protein that can be considered as the stator [16-20]. The rotor *vs.* stator subunits of the V-ATPase do not correspond exactly to those of the V_o *vs.* V_1 domains, because subunit a and d of V_o are part of the stator, and subunits D and F of V_1 are part of the rotor [21; 22].

1.1.1.1. V_1 : the catalytic domain

The V_1 domain contains eight different subunits (A–H) (**Table 1**), some of which are present in multiple copies.

	Subunit	Molecular Weight (kDa)	Yeast gene	Function
V_1	A	70	VMA1	Catalytic side, regulation
	B	60	VMA2	Interacts with A during catalysis
	C	40	VMA5	Peripheral stalk
	D	34	VMA8	Central stalk
	E	33	VMA4	Peripheral stalk
	F	14	VMA7	Central stalk
	G	13	VMA10	Peripheral stalk
	H	50	VM13	Peripheral stalk

Table 1: Subunits of the V_1 domain.

The V_1 domain contains three copies of each A and B subunits, two copies of the E and G subunits, one or two copies of subunit H and single copies of the remaining subunits [8; 23]. In V_1 , the A and B subunits are arranged in alternating positions of a hexamer of nearly 400 kDa, and ATP hydrolysis occurs at three catalytic sites, each located at one of the two

types of interface of the A and B subunits. These two subunits are homologous to the α and β subunits, of F-ATPase, with amino acid identities ranging from 20 to 25%, with the highest conservation in the nucleotide binding regions. The remaining V_1 subunits are distributed between one of two types of stalks - peripheral and central - that connect the catalytic head group (V_1) and membrane domains (V_o). These stalks have distinct functions in the rotary mechanism by which the V-ATPases couple ATP hydrolysis to proton transport. The central stalk serves as the axis of the rotor that couples the energy that is released from the hydrolysis of ATP to the rotation of a ring of proteolipid (*c*-type) subunits in V_o . The peripheral stalks serve to prevent rotation of the A_3B_3 head during ATP hydrolysis and therefore serve a stator function.

1.1.1.2. V_o : proton translocation across the membrane

The V_o domain contains six different subunits (**Table 2**). In yeast these subunits are *a*, *d*, *e*, *c*, *c'* and *c''* [23; 24].

	Subunit	Molecular Weight (kDa)	Yeast gene	Function
V_o	a	100	VPH1/STV1	Proton transport
	d	38	VMA6	Bridges V_o and V_1 rotor parts
	c	18	VMA3	Proton transport
	c'	18	VMA11	Proton transport
	c''	21	VMA16	Proton transport

Table 2: Subunits of the V_o domain.

The *c*-type subunits appear to be present in a stoichiometry of four *c*-subunits to one copies of *c'* and *c''* subunits each, that are arranged to form a ring ($c_4 c'_1 c''_1$) [15; 25], although $c_3 c'_1 c''_2$ assemblies are also reported [26]. The role of diversity of the *c*-ring is not known but it might be related to the regulation of the V-ATPase and the fact that, in different tissues, the *c*-ring appears in roles such as, *e.g.*, gap junctional and neurotransmitter-release channels, or parts of the membrane fusion machinery, that are unrelated to the V-ATPase activity [27-30]. The *c*, *c'* and *c''* subunits show homology to the *c* subunits of the F-ATPase (in which there are ~12 *c*-subunits), but appear to have undergone gene duplication, resulting in four transmembrane helices or five transmembrane helices for *c''* subunit [15; 26], rather

than the two transmembrane helices typically found in *c* subunits of F-ATPase, where each contains a unique proton-binding aspartic acid. In V-ATPase, each proteolipid subunit has a single buried glutamic acid located in transmembrane helix 4 (TM4) of subunits *c* and *c'* and helix 3 (TM3) of subunit *c''*. These Glu residues undergo reversible protonation during proton transport.

Subunit *a* is a 100 kDa protein crucial for proton transport. It has a hydrophilic N-terminal domain oriented towards the cytoplasmic surface and a C-terminal domain that contains eight or nine transmembrane helices. In TM7 of subunit *a*, there is a buried arginine residue that is absolutely required for proton transport [31]. Subunit *a* is the only yeast V-ATPase subunit that is present in multiple isoforms, encoded by the *VPH₁* and *STV₁* genes. They are usually assigned to the vacuole (*Vph1p*) and to the Golgi and endosomes (*Stv1p*) [32]. This suggests that the isoforms are responsible for enzyme localization.

The V_o domain also contains the tightly bound peripheral subunit *d* and a highly hydrophobic, 9 kDa polypeptide (subunit *e*) [24]. Subunit *d* is located on top of the ring of proteolipid *c* subunits, which provides a connection between the central stalk of V_1 and the proteolipid ring of V_o [33]. The *e* subunit is part of the final V-ATPase complex, both in yeast and in other eukaryotes, and is essential for its assembly and function, but nothing is known about its placement or function in the V_o sector [24; 34; 35].

1.1.2. Catalysis and ion transport coupled by a rotary mechanism in V-ATPase

The catalytic molecular rotary mechanism was first proposed for the F-ATPase by Boyer in the early 1980s [36; 37], later Nishi and Yoshida assumed that V-ATPase uses a similar rotary mechanism in catalysis, because of the structural and functional similarities with F-ATPase [6; 8].

The rotation of the central rotor subunits is a key feature of these enzymes in coupling ATP hydrolysis/synthesis to ion transport across the membrane. The catalytic site of F_1 is formed at the interface between the α and β subunits, with the majority of the catalytic residues residing in the β subunit. The minimum rotary unit of F_1 is the $\alpha_3\beta_3\gamma$ subcomplex, in which the central γ subunit rotates within the $\alpha_3\beta_3$ core by repeating a sequence of four steps, which are sub-

steps of a 120° step rotation [17; 38; 39]: (1) binding of ATP to a catalytic β subunit, (2) 80° rotation of the γ subunit, (3) cleavage of ATP and/or release of hydrolysis product(s), and (4) 40° rotation of γ . ATP hydrolysis in V-ATPase proceeds via the same 120° turn steps rotation mechanism where D and F subunits rotate relative to the A_3B_3 complex. Subunit *a* and the A_3B_3 hexamer are held in fixed positions relative to each other by the peripheral stator(s). Rotation of the proteolipid ring relative to subunit *a* performs the active transport of protons.

Subunit *a* provides a path for protons in the form of aqueous hemichannels, as previously proposed for the ATP synthase [40-42], and in the same time confer chirality on the direction of rotation. The cytoplasmically oriented hemichannel allows the proton to reach the buried carboxyl group on one of the proteolipid subunits [43]. Following protonation of this carboxylate, ATP-driven rotation of the proteolipid ring brings the protonated carboxyl group into contact with the lumenally oriented hemichannel. Interaction between the carboxyl group on the proteolipid subunit and a positively charged buried arginine residue in subunit *a* displaces the proton into the luminal hemichannel, thereby creating a deprotonated carboxylate available to bind another proton. It was shown that the TM7 of subunit *a* containing the critical arginine residue comes into close proximity to TM4 of subunits *c*, *c'* and TM3 of subunit *c''* that each contain a buried glutamic acid residue essential for proton transport [44; 45]. The different environments of the two hemichannels may cause different pKa values of the glutamic acid residue in the proteolipid. In this respect, a conserved arginine residue in one of the putative transmembrane helices of subunit *a* is critical for proton transport, and is thought to act by stabilising the glutamic acid residue favoring deprotonation in the luminal hemichannel.

In V-ATPase, the essential TM helices both in *a*- and the proteolipid subunits undergo helical swivelling (rotation about an axis through the centre of the helix) relative to each other, which is possibly coupled to catalysis. The V-ATPase specific inhibitors bafilomycin and concanamycin A having IC_{50} (concentration resulting in 50% inhibition) values in the nM range are thought to inhibit proton transport by blocking this helical swiveling [2].

To establish a study of the rotation of V-ATPase is difficult because it can be measured directly only if the enzyme is modified to a great extent. Therefore limited data are available for the rotational rate of the V-ATPase and in addition, most of them on bacterial

V-ATPase. For direct detection of the rotation beads, actin filaments, antibodies were attached to the protein by biochemical procedures in a few studies (**Figure 3**) [46-51].

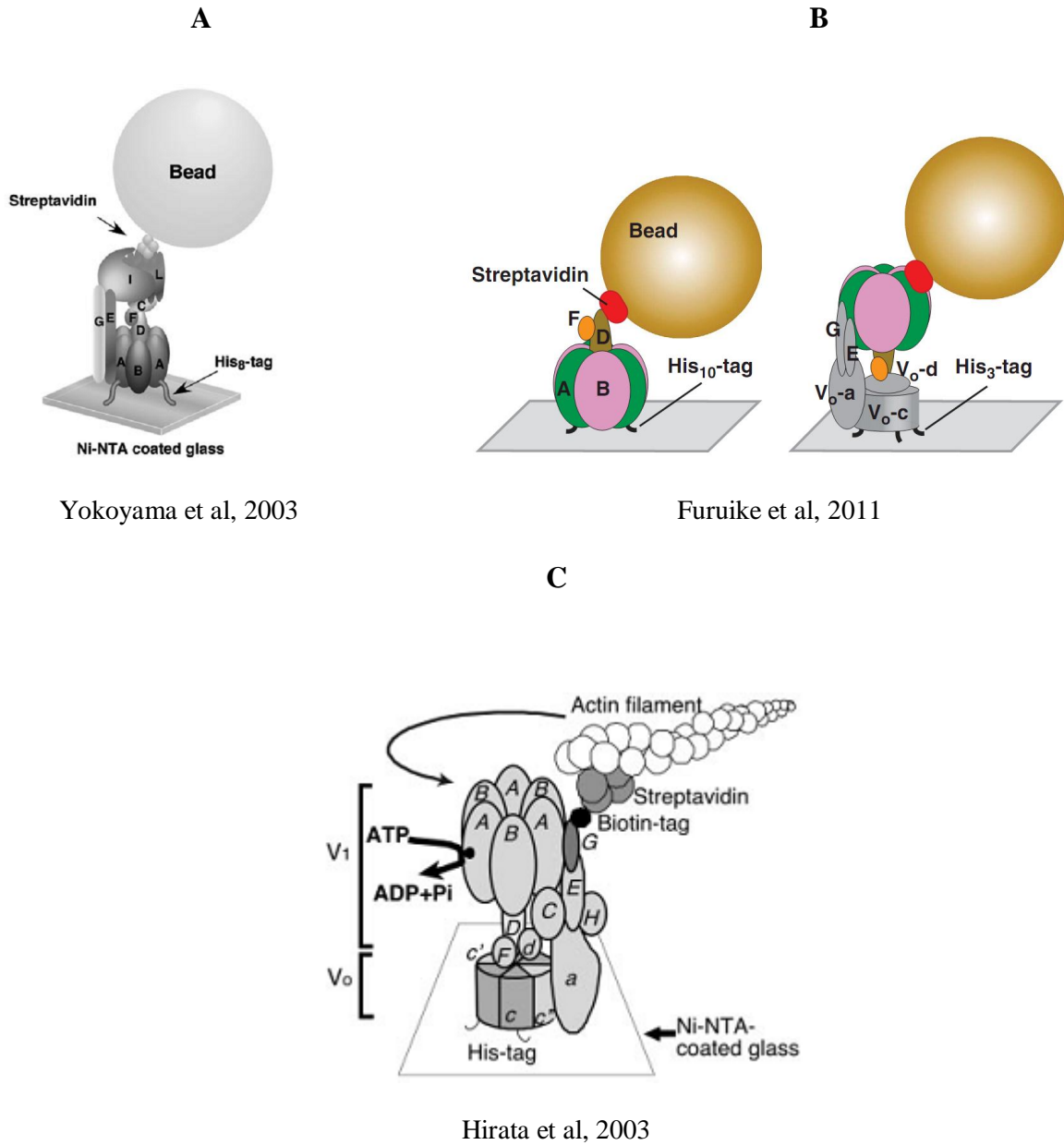


Figure 3: Rotation scheme of V-ATPase, carrying attached bead and actin filament: **A.** Rotation of V₀V₁ATPase of *Thermus thermophilus* (~3.0 rev/s at 4 mM ATP) [46]; **B.** Rotation of V₁ (~60 rev/s at 4 mM ATP) (left) and V₀V₁-ATPase (right) (~ 1-10 rev/s at 4 mM ATP) of *Thermus thermophilus* [51]; **C.** Rotation of V₀V₁-ATPase of yeast *Saccharomyces cerevisiae* [47].

Such modifications may add or remove barriers to the rotation that are not present in the native system, therefore the published rotation rates vary greatly in such studies [52-55].

Our objective for determination of the rotation rate was to work with native V-ATPase enzyme in a native membrane. As the above described studies are not possible in a native system, but because the ATP/rotation stoichiometry is known, one could assay the amount of the inorganic phosphate liberated due to the ATP hydrolysis by the V-ATPase in unit time and then relate this to the concentration of V-ATPase. This procedure also has its limitations. For example, it is not trivial, how to distinguish V-ATPase activity from those of other ATPases also present in the native membrane; how to determine V-ATPase concentration in the membrane, and in addition, what fraction of the V-ATPase present is actually active?

1.2. Structure and mechanism of Na,K-ATPase

1.2.1. Structure of Na,K-ATPase

The Na,K-ATPase or Na-pump belongs to a widely distributed class of P-type ATPases that are responsible for the active transport of a variety of cations across cell membranes [56]. The P-type nomenclature refers to the unique characteristic of these enzymes in forming a transient, phosphorylated aspartyl residue during the catalytic cycle. Accompanying the phosphorylation-dephosphorylation process these ATPases bind, occlude, and transport ions by cycling between two different cation-dependent conformations, called E_1 and E_2 conformational enzyme states (Post-Albers cycle) [57-59].

All P-type ATPases are multi-domain membrane proteins with molecular masses of 70–150 kDa. Both the carboxyl and amino termini are on the cytoplasmic side of the membrane, so they all have an even number of transmembrane segments (**Figure 4**).

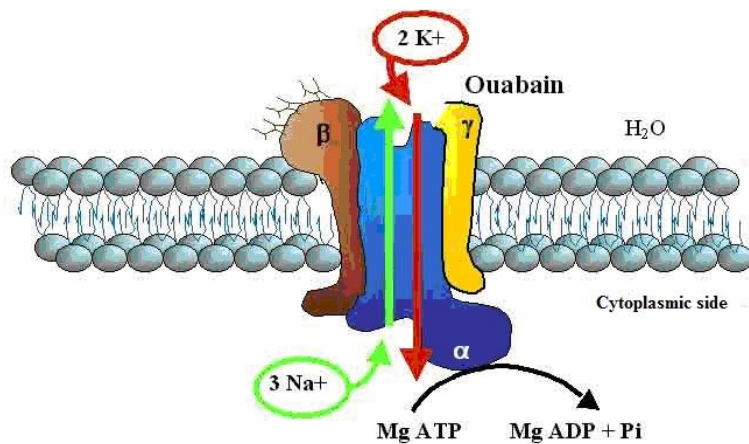


Figure 4: Structure of Na,K-ATPase. The three subunits of the pump are shown as follow: α - subunit in blue, β - subunit in brown and γ -subunit in yellow. The enzyme actively transports three Na⁺ out of the cell and two K⁺ into the cell for each molecule of hydrolyzed ATP. Na,K-ATPase activity is sensitive to ouabain, which is a potent and specific inhibitor of the enzyme.

The enzyme complex is formed by three polypeptide subunits (α , β , γ): the catalytic α subunit, which is composed by of approximately 1000 amino acid residues ($M_r = 100$ –112

kDa) with 10 TM helices and a large cytoplasmic domain; the auxiliary β subunit, which is composed of about 370 amino acids ($M_r = \sim 35$ kDa) with one transmembrane helix and a highly glycosylated extracellular domain; and a third regulatory subunit (7–17 kDa) that modulates the enzyme kinetics with one transmembrane helix and variable extra- and intracellular domains. The tissue-specific homologues of this third subunit belong to the FXYD protein family, which derives its name from a highly conserved signature sequence of amino acids (Phe-X-Tyr-Asp) preceding the transmembrane domain. Contrary to the β -subunit, the γ -subunit is not required for pump function [60].

The α subunit contains the functional sites for ATP, transported cations, and cardiac glycoside inhibitors. The β subunit is required for maturation and stability of the α subunit [61]. There are four α (α_1 , α_2 , α_3 , and α_4) and three β (β_1 , β_2 , and β_3) isoforms, expressed and regulated in a tissue- and development- specific fashion. The different combinations of $\alpha\beta$ isoforms exhibit somewhat different functional properties adjusted to the physiological requirements of the tissues [62].

1.2.2. Catalytic mechanism of Na,K-ATPase

The Na-pump establishes and maintains the high internal K^+ and low internal Na^+ concentrations. By using the energy from the hydrolysis of one molecule of ATP, it transports three Na^+ out in exchange for two K^+ that are taken in. The electrochemical gradient the Na,K-ATPase generates is critical in maintaining the osmotic balance of the cell, the resting membrane potential of most tissues, and the excitable properties of muscle and nerve cells. The reaction cycle of Na,K-ATPases is explained by the Post-Albers scheme [63; 64] or the E1/E2 theory (**Figure 5**).

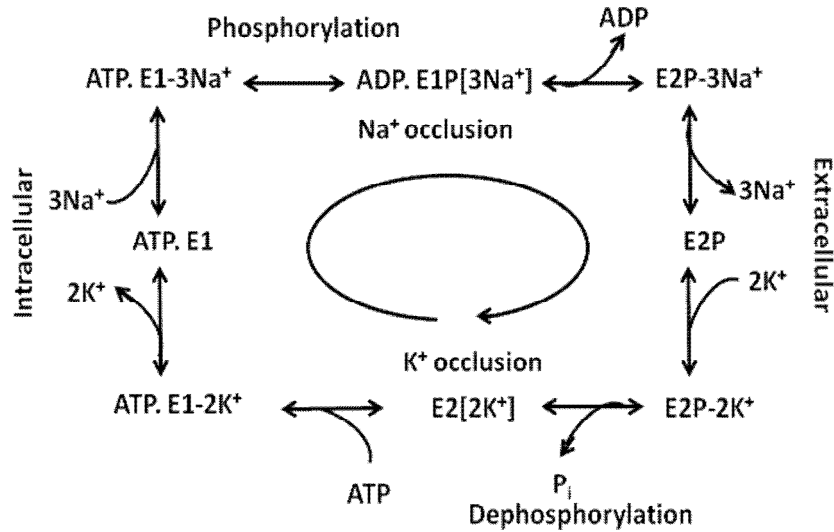


Figure 5: Operation of Na,K-ATPase pump. The circular arrow in the centre shows the direction of the physiological cycle driven by a high ATP/ADP ratio [65].

The pump is also named as $\text{E}_1\text{-E}_2$ ATPase, because it can exist in two main conformations: E_1 and E_2 . $\text{E}_1\text{-E}_2$ conformational transitions in the α -subunit change interactions between cytoplasmic domains and the cation sites in the intramembrane domain. These transitions couple the scalar processes of ATP binding, phosphorylation, and dephosphorylation to the vectorial extrusion of three Na^+ ions and uptake of two K^+ ions. The E_1 and E_2 conformations differ, for instance, in affinity for Na^+ and K^+ , sensitivity to ADP and ATP, intrinsic fluorescence, and sensitivity to proteolysis [66]. The E_1 conformation has a high affinity for sodium ions, can be phosphorylated by ATP, and presents the ion-binding sites to the cytoplasm. The E_2 conformation has a high affinity for potassium ions, can be phosphorylated by inorganic phosphate (P_i), and presents ion-binding sites to the extracellular aqueous phase. To ensure vectorial transport and to avoid channel-like short circuit, the system is expected to have two gates, one on the cytoplasmic side and the other on the extracellular side [67]. The two gates must operate in strict coordination, and the reaction cycle must contain a step in which both gates are closed so that the TM binding sites become inaccessible from either side of the membrane. The cytoplasmic gate is closed and locked by phosphoryl transfer to the aspartate only after three Na^+ are bound (i.e., transition from the E_1 to the E_1P state). In the E_1P state, bound Na^+ are occluded. E_1P is spontaneously transformed

into the low-energy “ADP-insensitive” E_2P intermediate, and during the transition to E_2 the extracellular gate opens and three occluded Na^+ ions are released to the extracellular side of the membrane (**Figure 5**). The E_2P form is able to bind two extracellular K^+ ions with high affinity, triggering hydrolysis of the aspartyl phosphoryl bond with resulting liberation of P_i . The extracellular gate is closed by the hydrolysis of the aspartylphosphate and locked in $E_2 \cdot 2K^+$. Then the protein in the form $E_2 [2K^+]$ is ready to initiate a new cycle. All of the steps in the reaction cycle are reversible, in the presence of Na^+ and K^+ gradients the enzyme can run backwards as well synthesizing ATP [68].

The conformational change of the enzyme upon the $E_1 \rightarrow E_2$ transition has been characterised by various methods [69; 70]. Differential scanning calorimetry (DSC) is a uniquely useful tool for studying the stability, heat of unfolding and domain structure of protein molecules. It was observed that for renal Na,K-ATPase, the $E_2(K)$ -form is more stable towards thermal denaturation as compared to the E_1 -form. Enzyme stability is a key concern in biological processes, so our focus was oriented onto the thermostability and unfolding of Na,K-ATPase and to factors affecting its destabilisation. We have chosen two different organisms, shark salt gland and pig kidney, that function at different temperatures. These animals belong to the poikilotherms and homeotherms, respectively, and therefore their Na,K-ATPase is adapted to function at different temperatures: about 8 °C for shark and 36 °C for pig.

As the three-dimensional structure of Na,K-ATPase is not resolved yet at atomic resolution, studying the domain structure can improve our knowledge on their structure and functioning.

2. The aim of the Work

We have chosen V-ATPase for studying because (i) its importance in several biomedical issues is gaining emerging recognition, (ii) membrane-bound molecular motors are in the forefront of biophysical research today and (iii) V-ATPase is optimally suited to our spectroscopy based structural biology approach, since its atomic resolution structure is still missing and its ATPase activity can be measured in native biological membranes. Our aim was therefore to use alternative approaches to study the structure-activity relationship and functioning of V-ATPase, more specifically:

- To optimise activity assay conditions (the choice of selective inhibitors, substrate concentration, reaction time, temperature) which ensure reliable measurement of steady state ATPase activity of V-ATPase being in its native membrane environment.
- To estimate the rotational rate of native V-ATPase from steady state activity measurements under standardised conditions.
- To develop a non-invasive approach, that is immune to uncertainties of pure activity based methods, in order to study the rotation rate of V-ATPase in its native state in the vacuolar membrane.

For these studies we chose to use yeast *Saccharomyces cerevisiae* cells as to our knowledge there are no data available for rotational rate of native, wild type V-ATPase in this organism.

Our membrane preparations from pig kidney and shark salt gland with increased concentration of Na,K-ATPase, served as ideal system to study the stability of the enzyme in organisms living at different temperatures. In case of Na,K-ATPase, we aimed to learn:

- The structural changes, and unfolding upon thermal denaturing by using differential scanning calorimetry.
- The effects of ionic strength and buffer compositions on its thermostability.

3. Materials and methods

3.1. Chemicals

The lyticase enzyme (crude, from *Arthrobacter luteus*), gramicidin A, N,N-dicyclohexylcarbodiimide (DCCD), N-Ethylmaleimide (NEM), carbonyl cyanide 4- (trifluoromethoxy)phenylhydrazone (FCCP), dodecyl sodium sulphate (SDS), DL-Dithiothreitol (DTT), sodium orthovanadate (Na_3VO_4), ascorbic acid, Ficoll-400, concanamycin A and bafilomycin were purchased from Fluka (Sigma-Aldrich), adenosine-5'-triphosphate disodium salt hydrate (Na_2ATP) was from Serva, D(-)-Sorbit, yeast extract, glucose and peptone were from Molar, sodium azide (NaN_3), ammonium molybdate tetrahydrate and Tris(hydroxymethyl)aminomethane (Tris) were from Reanal. All standard chemicals were of analytical grade purity.

3.2. Culture of yeast cells

Cells (*Saccharomyces cerevisiae* EMY 74.7) were grown in YPD medium (2% glucose, 2% peptone and 1% yeast extract) at 30 °C in a water bath shaker (New Brunswick Scientific Co.Inc) with continuous agitation. For vacuolar membrane vesicles isolation, overnight cultures were diluted to $\text{OD}_{600} = 0.1$ in 1L YPD media, and cells were harvested when cultures reached $\text{OD}_{600} = 0.8-1$.

3.3. Isolation of vacuoles and preparation of vacuolar membrane vesicles

Yeast vacuolar membrane vesicles were obtained by the method of Uchida et al. [71; 72] with some modification, as follows. Exponentially growing cells were harvested by centrifugation at 5400 rpm for 30 min at 4 °C in a GSA rotor (Sorvall rotors were used in a Sorvall RC-5C centrifuge unless stated otherwise). The pellet was resuspended in Tris buffer (100 mM Tris (pH 9.4), 10 mM DTT, 10 mM NaN_3) and centrifuged in a SS-34 rotor at 6500 rpm for 5 min at 4 °C. The pellet was resuspended in spheroplast buffer (1.5 M Sorbitol, 50 mM Tris (pH 7.2), 2 mM MgCl_2 , 10 mM NaN_3), which was supplemented with lyticase to

a final concentration of 1 unit/ml. The suspension was incubated at 30 °C for 90 min, with gentle shaking. Spheroplasts were cooled on ice and layered on the top of 5 ml 1.9 M sorbitol and centrifuged in an HB-4 rotor at 2100 rpm for 5 min at 4 °C. The recovered spheroplasts were washed by centrifugation (3800 rpm, 5 min at 4 °C) with 1 M sorbitol in the same rotor. The pellet was suspended in buffer A (10 mM Mes/Tris (pH 6.9), 0.1 mM MgCl₂, 12% Ficoll-400), supplemented with protease inhibitor cocktail tablet (Roche) (1 tablet/50 ml). The resulting mixture was homogenised with a Dounce homogenizer with 30 strokes and centrifuged at 5200 rpm for 5 min at 4 °C in an HB-4 rotor. For isolation of vacuoles 5 ml of supernatant was taken and transferred to an ultracentrifugation tube, 5 ml of buffer A was gently layered on top, and centrifuged in TH-641 rotor at 12500 rpm for 30 min at 4 °C (Sorvall Discovery 90SE by Hitachi ultracentrifuge). The white layer on the top of the centrifuge tubes represented the vacuoles. Vacuoles were recovered and converted to vacuolar membrane vesicles by diluting them ten-fold with buffer C (10 mM Mes/Tris (pH 6.9), 5 mM MgCl₂, 25 mM KCl) and centrifuged in AH-627 rotor at 15000 rpm for 30 min at 4 °C. The total protein concentration was determined with the Lowry assay [73] and the vesicles were stored at -80 °C in buffer C with 10% glycerol.

3.4. Light microscopy of yeast vacuoles

Transmitted light mode microscopy images of the vacuole suspensions were observed using differential interference contrast optics of Olympus IX81 inverted microscope. Images were captured with F-View 12-bit monochrome CCD camera using Olympus Cell-R software and UPlanSApo 60x oil immersion objective with a numerical aperture of 1.35.

3.5. Freeze-fracture electron microscopy of vacuolar membrane vesicles

Freeze-fracture electron microscopy was used for direct visualisation of the membrane structures evolved from the vacuoles. Glycerol was added to the vesicle dispersion as cryoprotectant at a final concentration of 20%. Addition of glycerol does not alter the bilayer structure, but inhibits the aggregation and ice crystal damage of the vesicles during the freezing process [74]. The gold sample holders used in freeze fracture were pre-incubated at

24 °C at the same temperatures as the samples. Droplets of 1-2 µl of the sample were pipetted onto a gold sample holder and frozen by plunging it immediately into partially solidified Freon for 20 s and stored in liquid nitrogen. Fracturing was performed at -100 °C in a Balzers freeze-fracture device (Balzers BAF 400D, Balzers AG, Vaduz, Liechtenstein). The replicas of the fractured faces etched at -100 °C for 30 s were made by platinum-carbon shadowing then cleaned with a water solution of surfactant and washed with distilled water. The replicas were placed on 200 mesh copper grids and examined in a Morgani 268D (FEI, Eindhoven, The Netherlands) transmission electron microscope.

3.6. Vacuolar H⁺-ATPase activity assay

To assay vacuolar H⁺-ATPase activity, 300 µg of total protein from the vacuolar membrane vesicles was used in 250 µl of assay mixture. Our activity assay and the use of inhibitors was based on earlier procedures [75-78], with modifications, as follows. The assay mixture contained the activity buffer (50 mM Mes/Tris (pH 7.0), 5 mM MgCl₂), 5 mM sodium azide (to inhibit mitochondrial ATPase), 0.2 mM ammonium molybdate (to inhibit acid phosphatases), 100 µM sodium orthovanadate (to inhibit plasma membrane H⁺-ATPase). The final concentration of the specific V-ATPase inhibitor concanamycin A (ConcA) was 1 µM. Vacuolar membrane vesicles were incubated in the activity buffer in the presence and absence of concanamycin A at room temperatures for 30 min. ATP hydrolysis was started by adding 2 mM Na₂ATP and the mixture was incubated at 30 °C for 20 min. The reaction was stopped by a solution containing 0.5% SDS, 2% H₂SO₄, 0.5% ammonium molybdate tetrahydrate and 10% of ascorbic acid. The acid was added to start colour development in the molybdate reaction which follows inorganic phosphate production, a product of ATP hydrolysis. The vesicle suspension was incubated in this stopping buffer at room temperature for 15 min. Absorbance was measured at 750 nm in a Thermo Spectronic (USA) spectrophotometer. The difference in the presence and absence of concanamycin A ($\Delta\text{OD} \pm \text{ConcA}$) gives the ATPase activity of V-ATPase. All data analysis and curve fitting was performed with the IGOR scientific graphing and data analysis program (WaveMetrics, Lake Oswego).

3.7. Vacuolar H⁺-ATPase under oscillating electric field

In these experiments, V-ATPase activity was measured as above, but with some modifications: 300 µg of total protein of vacuolar membranes vesicles was used in the assay in the presence and absence of 2 µM concanamycin A. The ATP hydrolysis reaction was started with 2 mM Na₂ATP and incubated at 20 °C for 10 min. During this time the sample was exposed to alternating (AC) electric field, using platinum wires as electrodes. Before starting the measurement control V-ATPase activity values were determined, using the same experimental condition but without the electric field. After 10 min the sample suspension was transformed from the cuvette into a tube and the reaction was stopped. After 15 min of incubation at room temperature the absorbance of liberated inorganic phosphate was measured at 750 nm. The alternating sinusoid-wave peak-to-peak voltage on the electrodes was 15 V and a series of low to high frequency (between 1 Hz and 10 kHz) were applied. The waveform, amplitude, and frequency of the AC field across the two electrodes were monitored directly on an oscilloscope (Tektronix TDS 210, two channel digital real time oscilloscope) [79; 80].

3.8. Na,K-ATPase enzyme preparations

The Na,K-ATPase enzymes were provided by M. Esmann and his laboratory (Arhus, Denmark) where the purification of the enzymes was performed. The procedure used was briefly as follows. The Na,K-ATPase membranes from the pig kidney dark red outer medulla and shark salt gland were prepared according to the method of Skou and Esmann [81], omitting the saponin treatment. Pig kidney microsomal membranes was prepared by treatment with SDS and purified by differential centrifugation [82; 83]. Shark salt gland microsomal membranes were treated with deoxycholate to make membrane vesicles leaky (omitting saponin) and purified by differential centrifugation. The shark enzyme was stored at a total protein concentration of about 5 mg/ml in 20 mM histidine and 25% glycerol (pH 7.0) and the pig kidney enzyme at a total protein concentration of about 4 mg/ml in 20 mM histidine, 250 mM sucrose and 1 mM EDTA (pH 7.0). The α- and β-subunits of the Na,K-ATPase have molecular weights of 112 kDa and 35.5 kDa, respectively, for both proteins; these subunits

constitute 70% of the total protein of the shark preparation and 60-70% of that from pig kidney. Protein concentrations were determined using the Lowry method [73]. The specific activity of both enzyme preparations was approximately 30 $\mu\text{mol ATP hydrolysed/mg protein/min}$ at 37 °C [84].

3.9. Sample preparation for differential scanning calorimetry

Purified membrane preparations were diluted with 1 or 20 mM histidine (pH 7.0 at 20 °C) to a final concentration of ca. 0.1 mg/ml. The sample was either incubated for 1 h at 20 °C and centrifuged at 4 °C for 2 h (20,000 rpm in a Beckman Ti70 rotor) or immediately subjected to centrifugation for 2 h at 4 °C. The pellet was resuspended in the same buffer (at a protein concentration of ca. 2.4 mg/ml) and used for DSC experiments.

3.10. Differential scanning calorimetry

DSC measurements were performed using a VP-DSC calorimeter, with 0.5 ml sample and reference cells, from MicroCal, LLC (Northampton, MA). The instrumental baseline was determined before each sample scan, by filling both sample and reference cells with the buffer used for the membrane samples, and using the same scanning parameters. Samples were scanned between 5 and 95 °C, at a rate of 1 °C/min, using the passive feedback mode of the VP-DSC instrument. Immediately after completion of the heating scan, a down-scan from 95 to 5 °C was performed at the same 1 °C/min rate. Reversibility and repeatability of the unfolding process was checked by this down-scan and a second up-scan, respectively. Before the start, and between repeated heating cycles, the samples were allowed to equilibrate for 30 min at 5 °C. The pH of the sample buffer decreased from 7.0 at 20 °C to about 6.7 at 50 °C.

Heat capacity data were corrected for the instrument baseline, and normalised for scan rate and protein concentration. Excess heat capacity profiles were analysed by using the software provided with the instrument. A progress baseline was fitted to each profile and subtracted, by selecting appropriate pre- and post- transitional segments. The total heat of denaturation (ΔH_{tot}), and the main transition temperature (T_{m}) were estimated by integration of the first unfolding endotherms in the range of the transition at the specific buffer condition. The number of components, their heat of denaturation (ΔH_{d}) and transition temperature (T_{d})

were estimated by fitting the thermogram in this range by a model of independent two-state transitions.

4. Results and discussion

4.1. Morphology and function of yeast *Saccharomyces cerevisiae* vacuoles and vacuolar membrane vesicles

The yeast vacuole is the site of storage of phosphate, selected amino acids, metals, and selected toxins. In addition, it helps buffering the pH of the cytoplasm and is important in water and ion homeostasis. Therefore, the vacuole plays multiple roles in the response to cellular stresses. Their sizes and forms can be different and one cell can contain more than one vacuole (**Figure 6**).

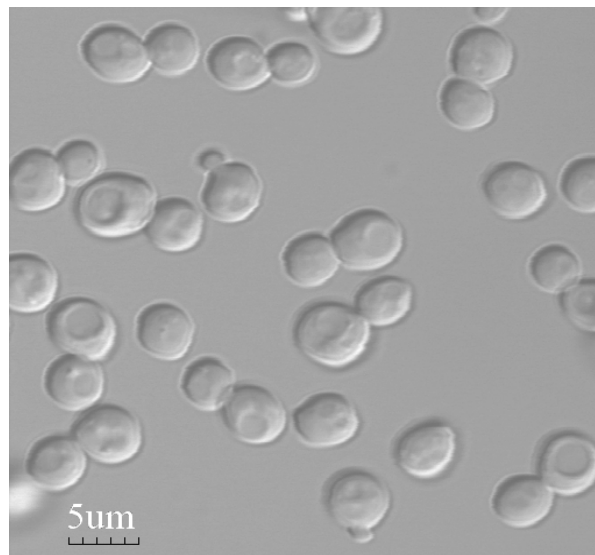


Figure 6: Morphological image of wild type yeast *Saccharomyces cerevisiae* cells with confocal laser scanning microscopy (image taken by F.Ayaydin).

Intact vacuoles were not used in our activity assay measurements because of their instability and being in an osmotic condition that is not optimal for the chemical compounds to react. To ameliorate the condition we applied osmotic shock on vacuoles, by which they were converted to vacuolar vesicles. With this procedure we also removed the loosely bound membrane proteins, decreased other ATPase activities of sources different from V-ATPase, thus increasing the specificity of our measurements. To visualise and to reveal vacuoles and

vacuolar membrane vesicle's sizes and shapes we used the Olympus Cell-R fluorescence microscope and freeze fracture electron microscopy (**Figure 7**).

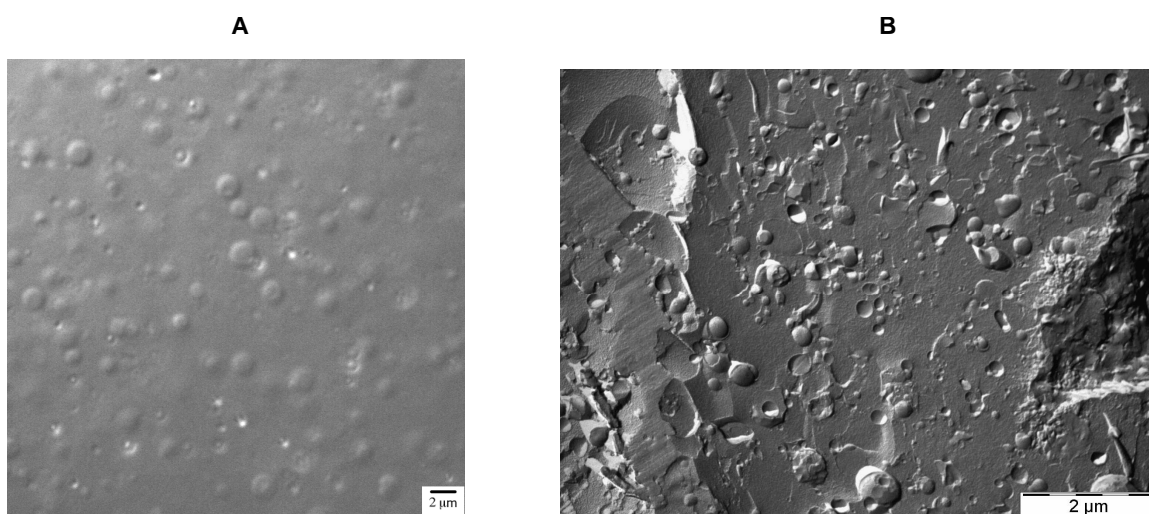


Figure 7: (A) Bright field transmitted light microscopy images of yeast *Saccharomyces cerevisiae* vacuoles using differential interference contrast configuration and 60x oil immersion objective (image taken by F. Ayaydin); and (B) Freeze fracture electron microscopy images of *Saccharomyces cerevisiae* vacuolar membrane vesicles fixed with glycerol (image taken by A. Bóta and Z. Varga).

From the freeze fracture images we were able to calculate the average size of vesicles present in our preparation. Each vesicle was counted and analysed with the image processing and analysis program (ImageJ). From the result we determined the average diameter of the vesicles (**Table 3**).

Count	Total Area (nm ²)	Average Size (nm ²)	Average diameter (nm)
471	18888924	40100±2300	226±4.7

Table 3: Particle analysis of vacuolar membrane vesicles. Average values are given with ± SEM.

We tested the functionality of our vacuolar vesicles with a biochemical assay by measuring the activity of V-ATPase in the presence and absence of specific inhibitors and different membrane protein inhibitors after a 20 min incubation of these vacuolar vesicles at 30 °C, in the presence of 2 mM Na₂ATP and 5 mM MgCl₂ (**Figure 8**). Because the substrate of the reaction is MgATP, and MgCl₂ was in excess relative to Na₂ATP, the substrate concentration was close to 2 mM (at least at the beginning of the reaction).

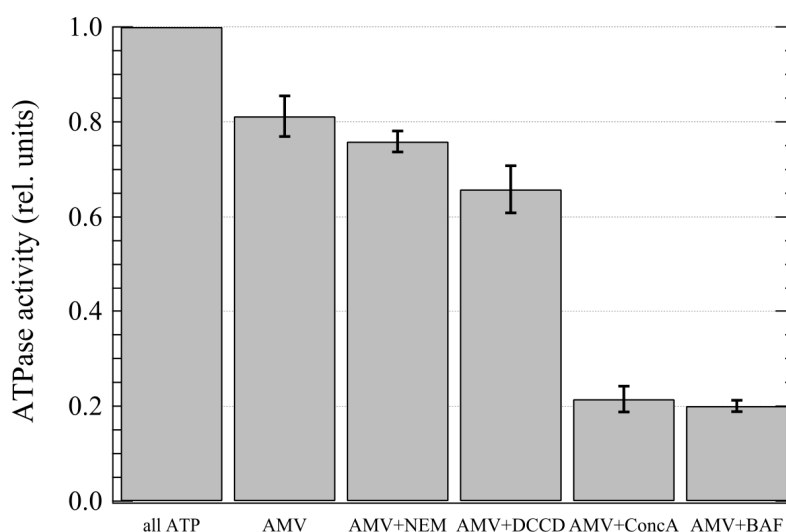


Figure 8: Comparison of ATPase activities of yeast vacuolar vesicles in the presence and absence of different ATPase inhibitors. ATP hydrolysis was stopped after 20 min of incubation at 30 °C in the presence of 2 mM Na_2ATP and 5 mM MgCl_2 and the medium was assayed for inorganic phosphate, in all cases. Abbreviations: all ATP, no inhibitors; AMV, 5 mM Na-azide + 0.2 mM molybdenate + 0.1 mM vanadate; AMV + NEM, as AMV plus 2 μM n-ethyl-maleimide; AMV + DCCD, as AMV plus 2 μM di-cyclohexyl-carbodiimide; AMV + Conc A, as AMV plus 1 μM concanamycin A; AMV + BAF, as AMV plus 1 μM bafilomycin. Results are normalised to the same “all ATP” activity. Bars indicate averages, errors mean a range of \pm standard deviation ($n = 3$). Corresponding activities of blank (no vesicles, no ATP, no inhibitor) and no ATP (no Na_2ATP , no inhibitor) samples were 0.0147 ± 0.0006 and 0.0253 ± 0.0025 , respectively (not shown).

ATPase activity was set to 100% when no inhibitors were present in the preparation (*all ATP*). The difference in ATPase activity in the presence and absence of 1 μM concanamycin A (a potent and specific V-ATPase inhibitor [85]) (*AMV \pm Conc A*) yields the ATPase activity of V-ATPase. Typically 60% of the total ATPase activity comes from V-ATPase in these vesicular preparations. Bafilomycin has similar effect as concanamycin A as they are part of the plecomacrolide-defined class of macrolide antibiotics (**Figure 9**).

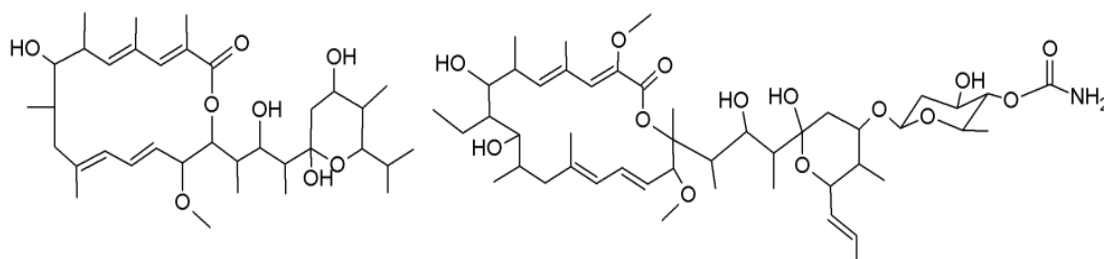


Figure 9: Structure of bafilomycin (16- membered laktone ring, left) and concanamycin A (18- membered laktone ring, right).

The exact binding site and the way of action of these inhibitors are not yet known. In some studies, it is described that they inhibit V-ATPase activity by binding to the proteolipid subunit *c* of the proton-translocating V_o complex [86] while other studies seem to confirm the interaction with subunits *c'*, *c''* and *a* of the yeast V-ATPase [87].

The ‘other’ inhibitors removed only about 20% of the total ATPase activity. Di-cyclohexylcarbodiimide, which inhibits proton translocation also in the related F-ATPase, was more potent, but the most potent inhibitors were, as expected, concanamycin A and bafilomycin.

In this complex enzyme system self-inhibitory effect can appear from improper use of substrate concentration. In **Figure 10** we tested the substrate concentration in a wide range. This was done by measuring the absorbance (at 750 nm) for inorganic phosphate liberated by ATP hydrolysis in the vacuolar vesicles, and assayed after 20 min incubation at 30 °C, as a function of the concentration of exogenously added Na_2ATP , both at fixed (5 mM) MgCl_2 concentration (circles) or when it was set to 2-fold that of the Na_2ATP (squares).

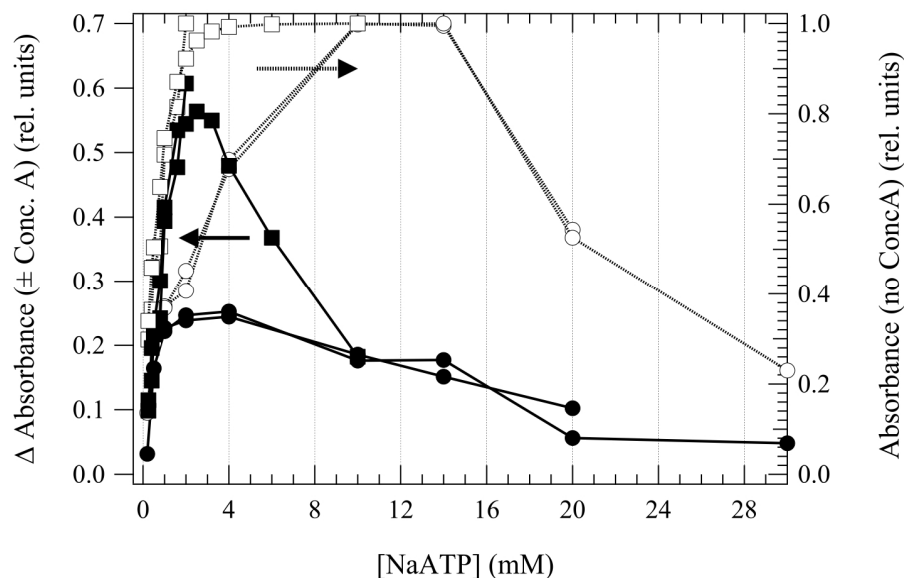


Figure 10: Relative absorbance (at 750 nm) for inorganic phosphate (P_i) liberated on ATP hydrolysis by yeast vacuolar vesicles, and assayed after 20 min incubation at 30 °C, as a function of the concentration of exogenously added Na_2ATP (open symbols, right y-axis). The data are normalised to the same maximum absorbance. Delta absorbance is the difference between the above normalised absorbances in the absence and presence of 1 μM of the specific V-ATPase inhibitor concanamycin A (solid symbols, left y-axis). $MgCl_2$ concentration was either kept constant at 5 mM (circles) or was set to 2-times the Na_2ATP concentration (squares, data measured by P. Petrovski). Each dataset, at constant or varying concentration of $MgCl_2$, was measured twice from independent cell cultures.

The figure shows the ATP concentration dependence of the whole system, with no inhibitor (open symbols) and that of V-ATPase alone (solid symbols), obtained from the difference in absorbance with and without 1 μM concanamycin A. The whole system saturates at ~ 2 and ~ 10 mM Na_2ATP , in the excess and fixed $MgCl_2$ concentration cases, respectively, and the production of inorganic phosphate decreases at high substrate concentrations (only measured for the latter case). The reason for the downward shift of the saturation lies most probably in the different ATP/Mg stoichiometries in the two cases. This, however, does not influence the point of maximum activity of the V-ATPase (at 2–3 mM Na_2ATP), because at that concentration even 5 mM $MgCl_2$ can be considered as in excess. We do not know the exact reason for the drop in activity, either in the case of the V-ATPase or the whole system, at high substrate concentrations. One can speculate that, due to spontaneous $ATP \rightleftharpoons ADP + P_i$ dissociation and possibly even ADP impurities in the ATP stock, the ADP concentration might reach a level at which it significantly inhibits ATPases. Nevertheless, the choice of 2 mM Na_2ATP and 5 mM $MgCl_2$ ensures that inhibition of this kind is negligible, and that the

V-ATPase is running at the highest speed with respect to substrate concentration, at least at the beginning of the incubation period, (which also needs to be standardised in order to avoid consumption of all substrate during the reaction).

In this complex membrane system, the reaction time of ATP hydrolysis must be optimised too: the time should be short enough to prevent consumption of the substrate but long enough to obtain a conveniently high yield of P_i , liberated by V-ATPase. **Figure 11** shows the time-dependence of (Δ) absorbance obtained as the difference between the absorbances of assayed inorganic phosphate liberated by ATP hydrolysis by yeast vacuolar vesicles in the absence and presence of $1 \mu\text{M}$ of the specific V-ATPase inhibitor concanamycin A, in the presence of exogenously added $2 \text{ mM Na}_2\text{ATP}$ and 5 mM MgCl_2 .

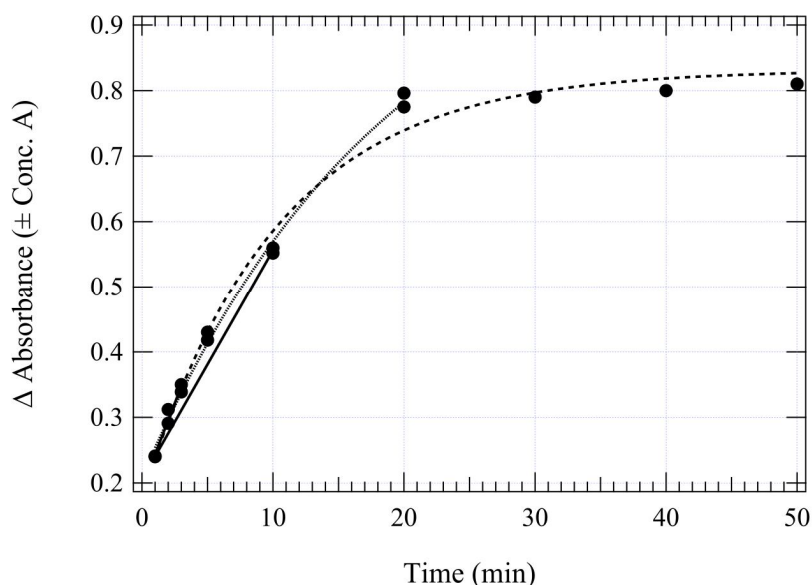


Figure 11: Time dependence of hydrolysis assay. The dotted and dashed lines are single exponential fits over the 0-10 min and 0-50 min regions, respectively, and are shown just as guides for the eye. The solid line over the 1-3 min time interval is a linear fit to the first 5 points. The solid line over the 0-10 time interval connects the means of the two data points at 1 and 10 min. Over the first 1-20 min region, absorbance was measured twice from independent cell cultures.

As shown above the absorbance difference of $\pm (1 \mu\text{M})$ concanamycin A measures phosphate liberated exclusively by V-ATPase. Since the substrate concentration decreases during the reaction, the rate of ATP hydrolysis by V-ATPase decreases monotonically too. The semi-kinetic curve does not follow a single exponential, as demonstrated by the poorness of the single exponential fit over the whole incubation period. The reason is, that the product, ADP,

inhibits the enzyme. Obviously, the fit over the first 20 minutes, where the concentration of the product is much lower, is closer to a single exponential. It should be noted that the exponential fits are presented just for the visualisation and they were not used in this study for any further analysis. Based on this experiment, the duration of the reaction was chosen to be 10 min. Comparing the $\Delta A/\Delta t$ slope of the fit to the first 5 points (onset slope) with the slope of the line connecting the points at 1 and 10 min (straight lines in Fig. 11), one can estimate the rate of ATP hydrolysis at the beginning of the incubation period if the mean is known. The ratio between the two slopes is 1.48.

Under the above optimised conditions of the V-ATPase activity assay in the native membrane, including spectrophotometric calibration for inorganic phosphate (**Figure 12**) one can determine the concentration of V-ATPase and using the specific inhibitor concanamycin A. The enzyme concentration, which is needed to convert this data into revolutions of the rotor per second, can be determined from the inhibitor titration curve (Fig.12) fitted with the appropriate binding equation, because the inhibitor concentration is known and the shape of the curve depends (differently) on the enzyme concentration and the dissociation constant for enzyme-inhibitor binding.

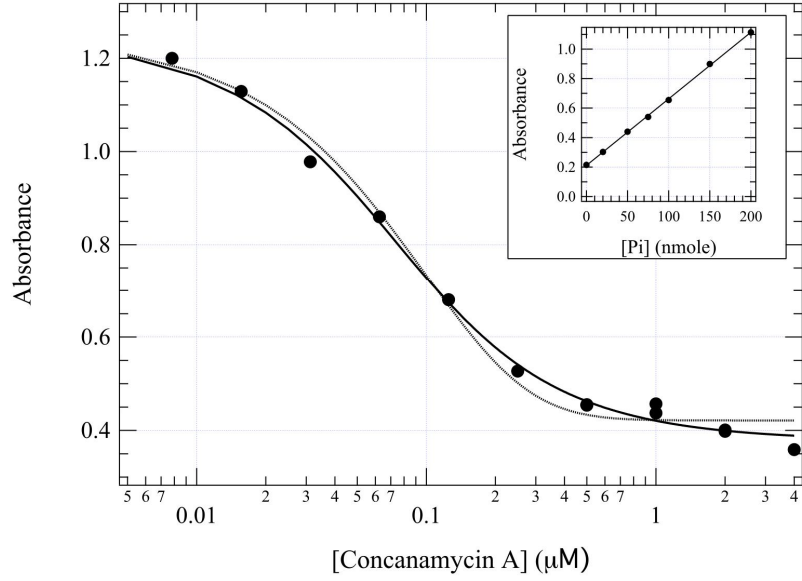


Figure 12: The absorbance (at 750 nm) of inorganic phosphate (P_i) liberated on ATP hydrolysis by yeast vacuolar vesicles, as assayed after 10 min incubation at 20 °C in the presence of 2 mM Na_2ATP (and 5 mM MgCl_2), as a function of the concentration of the specific V-ATPase inhibitor, concanamycin A. Three points at zero inhibitor are invisible because of the logarithmic axis. The solid curve is a released fit according to the quadratic binding equation assuming a single binding site per monomeric enzyme. The dotted curve is a fit according to the model with 5 binding sites per monomer V-ATPase enzyme. The inset shows the corresponding photometric calibration of absorbance versus the molarity of exogenously added inorganic phosphate $[P_i]$, in the same preparations, same reaction volume and under the same conditions as the titration with the inhibitor, except that no Na_2ATP was added (data measured by P. Petrovski).

It is assumed below that all inhibitor molecules (I) are active and that all V-ATPase molecules are active if no inhibitor is bound but are inactivated when at least one inhibitor is bound. In this case the data in Fig. 12 should follow the equation:

$$A(I_t) = A_0 - \Delta A * (1 - P_f / P_t), \quad (1)$$

where $A(I_t)$ is the absorbance considered as a function of the total inhibitor concentration, I_t . A_0 is the absorbance in the absence of inhibitor, ΔA is the difference in absorbance at zero and saturating concentration of the inhibitor. P_t is the (total) enzyme concentration and P_f is the concentration of the enzyme without any inhibitor bound (the indices t , f and b mean total,

free and bound sites or molecules, respectively, and the symbols indexed are the corresponding concentrations). The relevant binding equations need to be solved in order to derive P_f/P_t as a function of I_t . The binding equation with the corresponding concentration is:

$$B_f * I_f = I_b * K_d , \quad (2)$$

where K_d is the intrinsic dissociation constant for inhibitor binding to a single, independent binding site. Because $B_f = P_t - I_b$ and $I_f = I_t - I_b$, it follows that:

$$(P_t - I_b) * (I_t - I_b) = I_b * K_d \quad (3)$$

Substituting, the solution of eq. (3) into (1), one obtains that

$$A(I_t) = (A_0 - \Delta A) + \Delta A * (P_t - I_t - K_d + ((I_t + P_t + K_d)^2 - 4 * P_t * I_t)^{1/2}) / (2 * P_t) , \quad (4)$$

which is the expression needed for fitting the single binding site model to the data in Fig. 12. In these fits, I_t is the independent variable and P_t , K_d and ΔA are fitting parameters. From the fit the absolute amount of inorganic phosphate corresponding to ΔA is liberated by 44.9 ± 31.6 nM V-ATPase.

The inset shows the phosphate calibration where the slope of the linear regression is $0.00452 \Delta OD/nmole$ Pi, from which the concentration of Pi liberated by V-ATPase is $770 \mu M$. Taking the ratios of the mean concentrations one concludes that in 10 min ca. 17000 Pi molecules, *i.e.*, approximately 30 per second, were liberated by each V-ATPase molecule. Current understanding of the V-ATPase catalysis assumes hydrolysis of three ATP molecules in a complete 360° rotation cycle [88], which means that the rotation rate in V-ATPase in our vacuolar membrane vesicle system is ~ 10 Hz at $20^\circ C$, which from the time-dependence of the activity (Fig.11), extrapolates to ~ 14 Hz at the beginning of the reaction. The data is compatible only with a single binding site per monomeric enzyme as for multiple binding site models we got physically meaningless values (not shown). The above rates are low limit estimates, because the activity of the inhibitor is most probably less than 100%, and it is also

very likely that not all enzymes are active in the vesicle preparations, and we do not know if the inhibitor binds to otherwise already inactive V-ATPase.

4.2. Rotary mechanism of vacuolar H⁺-ATPase under oscillating electric field

To investigate the rotary mechanism of vacuolar H⁺-ATPase, we used vacuolar membrane vesicles isolated from wild type *Saccharomyces cerevisiae* yeast cells. Almost 60% of the total ATPase activity comes from V-ATPase in these preparations (see fig.8). In order to test any temporal periodicity in the vesicular preparations due to the rotary mechanism of the V-ATPase, we developed a non-invasive method (**Figure 13**), which did not need any genetic or chemical modification of the enzyme. In addition, V-ATPase remained in its native membrane environment. This approach is also immune to uncertainties of the above steady state activity method. Using a fix voltage (15 V) and a variable range of frequencies we measured the effect of oscillating electric field at 20 °C for 10 min in the presence and absence of concanamycin A, under the previously standardised conditions.

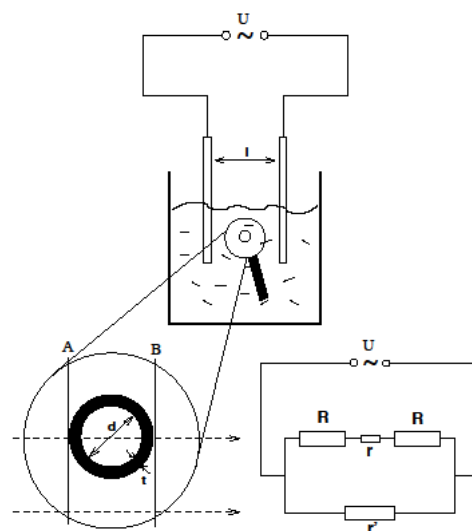


Figure 13: Experimental setup for V-ATPase activity in oscillating electric field (sample arrangement and the analogous electric circuit). Alternating oscillating electric field was applied on the sample suspension for 10 min at 20 °C. ATP hydrolysis was initiated by 2 mM Na₂ATP. The measurement was repeated in the presence and absence of 2 μM concanamycin A. The transmembrane electric field was $|E_m| = \sim 562.5$ V/cm.

The presence of the AC field reduced the ATPase activity of V-ATPase over a wide frequency region except for a narrow band, where a resonant like effect was first observed at 88.3 Hz (**Figure 14**). In this resonant region the ATPase activity reaches or exceeds that of the control (no AC) level. (For different vacuolar membrane vesicle preparations the centre-frequency of the resonant region varied between 87-94 Hz).

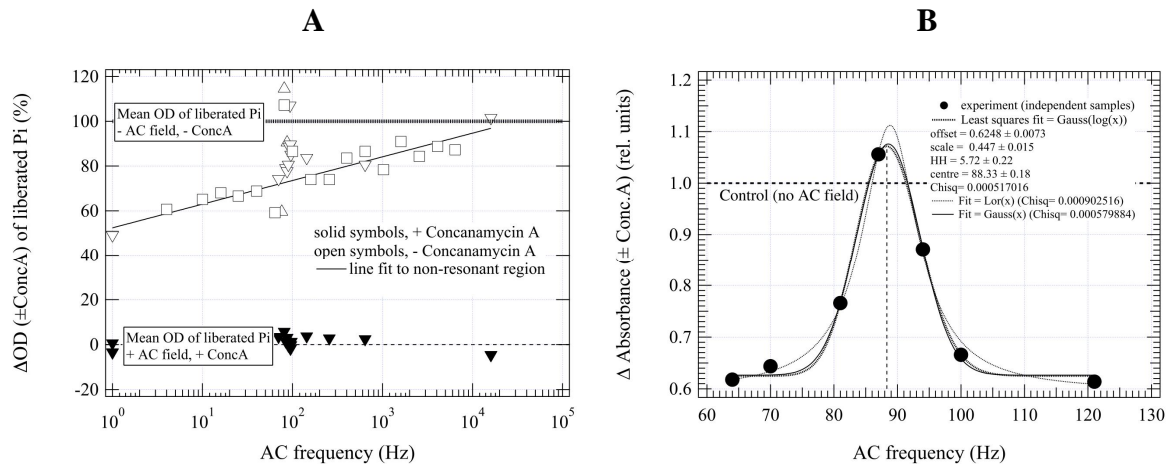


Figure 14: Normalised V-ATPase activity as a function of the frequency of AC field over a wide (A) and narrow (B) frequency region. In panel (A) different open symbols mean different series of preparations and black symbols (also in panel (B)) indicate one selected preparation. OD values were normalised such that mean ODs of + Conc A,+ AC and – Conc A,- AC values were set to 0 and 100% respectively.

We could prove that the effect is related to a transmembrane potential: in the presence of different concentration of FCCP and gramicidin A, which are known to make pores in the lipid membranes, the resonant activity peak diminished (**Figure 15**).

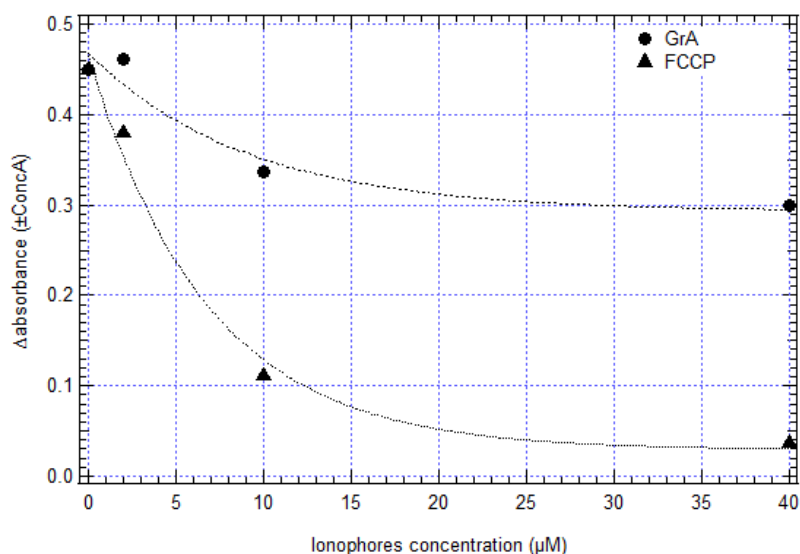


Figure 15: The height of the resonant peak (see Fig. 14(B) - narrow frequency) as a function of the concentration of FCCP and gramicidin A added to the yeast vacuolar vesicle preparations, in an ATP hydrolysis assay performed at 20 °C, after 10 min incubation. Delta absorbance was obtained as the difference of absorbance between the absence and presence of the specific inhibitor concanamycin A.

It is apparent that gramicidin A is less effective, maybe because it forms fewer membrane pores.

4.3. The two-channel model

The only complete explanation for all the above observations is that the AC field interacts with the transmembrane proton movements. How rotation of the rotor mediates the linear transfer of H^+ across the membrane is illustrated in **Figure 16**, based on the models proposed for the F-ATPases [43; 89; 90] and V-ATPases [91; 92]. The inner half channel of subunit *a* is thought to allow cytoplasmic H^+ to access and bind to one subunit of the *c*-ring. After the nearly 360° rotation of the *c*-ring, H^+ can unbind and exit the membrane through the outer half channel.

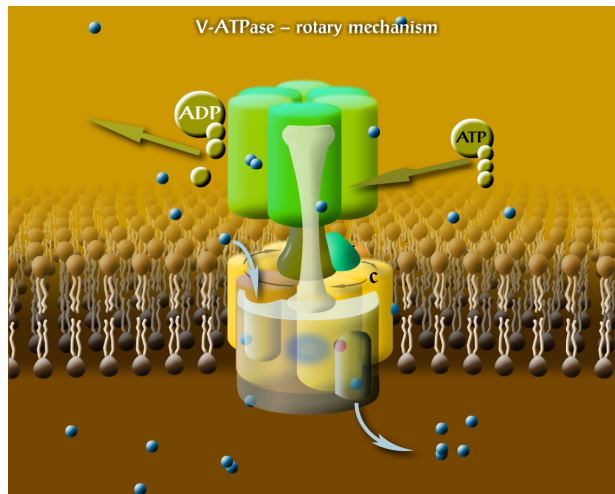


Figure 16: V-ATPase rotation mechanism. Hydrolysis of ATP brings rotation of the central shaft together with the *c*-ring of the V_0 complex. Rotation of the *c*-ring transmits H^+ from the inner half channel to the outer half channel via an intermediary H^+ binding step to one subunit *c*. Each subunit *c* carries one proton, when in contact with lipids (Not all subunits are shown).

Due to the geometry of the hydrophilic proton channels between subunit *a* and *c* and the proton binding sites on the *c*-ring it follows that there are phases within a rotor step where a proton can or can not move along the membrane normal (**Figure 17**) [91].

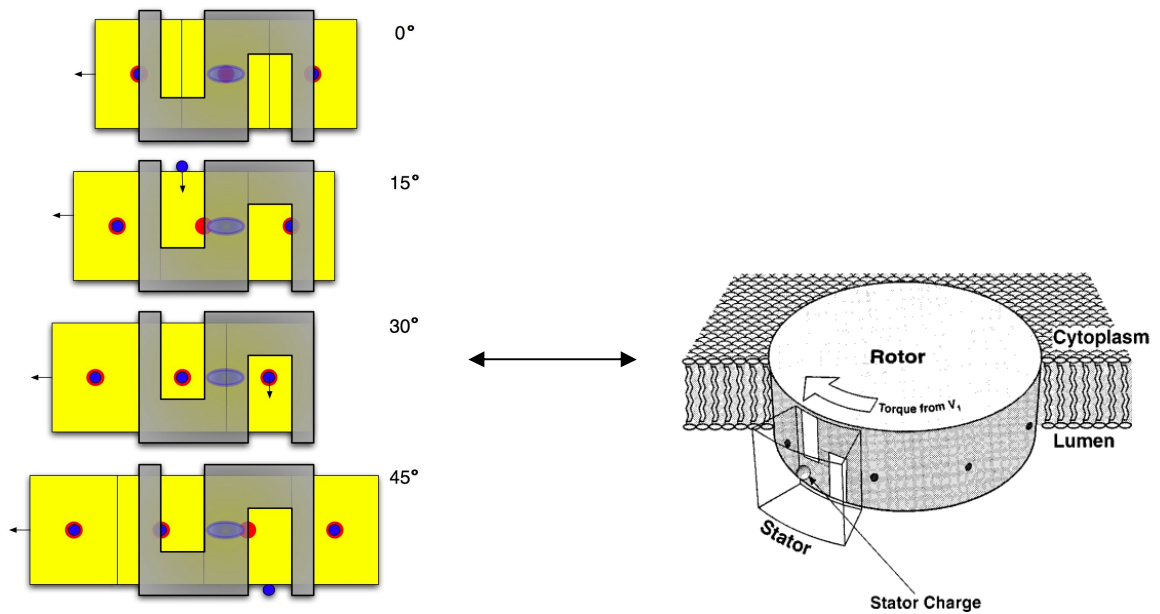


Figure 17: Two-channel model of rotor-stator assembly. The basic, 60 degrees cycle of the rotor and proton movements in V-ATPase (equivalent of rotation by one subunit *c*), according to current understanding of the rotary mechanism. The subunit *c* ring is yellow and the stator (subunit *a*) is grey. The unique Glu residues are red and protons are blue as is the unique Arg residue of subunit *a*.

If these phases are comparable in time then a matching AC frequency does not inhibit proton translocation or may even enhance it (**Figure 18**), whereas too slow or too fast AC will both inhibit it (very high frequencies are less inhibitory because the AC periodicity gets shorter than the kinetics of the system). So, according to the most accepted model of the rotary mechanism in V-ATPase, the resonance frequency of 88.3 Hz is that of the 60° steps of the rotor, equivalent of 14.7 Hz of the full 360° rotation. This is in a very good agreement with the lower limit estimate of 10 Hz obtained from the concanamycin A titration experiment, under the very same conditions except for the presence of the AC field.



Figure 18: Snapshots from our animated model to explain the effect of oscillating (AC) trans-membrane electric field on the ATP hydrolysing activity of V-ATPase (case: the frequency of the AC field matches the intrinsic rate of the 60 degrees rotor steps). Left: The phase of the rotary cycle, with vertical proton movement in the hydrophilic channels in the subunit *c-a* interface. If the AC field is in the right phase, it enhances proton movement, otherwise it acts against it. Right: The phase of the rotary cycle without vertical proton movement. In this rotor phase the AC field has little effect, even in the "wrong" phase, because they are not in the channels to move. (Excerpt from our interactive computer animation based on our current understanding on the V-ATPase bio-engine. Only the rotor (yellow) and stator (green) subunits are shown.)

4.4. Differential scanning calorimetry of shark Na,K-ATPase containing membranes

Whereas native yeast vacuoles contain a relatively high concentration of V-ATPase, we had to apply special procedures in order to prepare pig and shark membrane dispersions enriched in Na,K-ATPase. These membrane preparations were optimal for structural stability studies, such as thermal unfolding measurements.

With the use of DSC we aimed to test the factors affecting Na,K-ATPase enzyme stability by different ionic strengths under various preparation conditions. **Figure 19** shows the DSC heating scans for membranous shark Na,K-ATPase preparations, under different conditions.

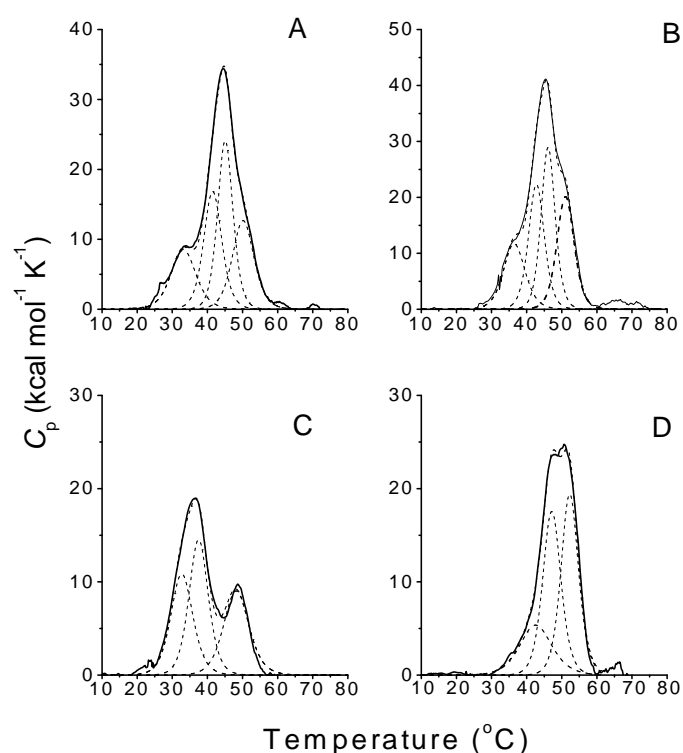


Figure 19: Excess heat capacity functions of membranous Na,K-ATPase from shark salt gland, after baseline subtraction. (A) Enzyme in 20 mM histidine, centrifuged for 2 h at 4 $^{\circ}\text{C}$. (B) Enzyme in 20 mM histidine, preincubated for 1 h at 20 $^{\circ}\text{C}$, prior to centrifugation for 2 h at 4 $^{\circ}\text{C}$. (C) Enzyme in 1 mM histidine, centrifuged for 2 h at 4 $^{\circ}\text{C}$. (D) Enzyme in 1 mM histidine, preincubated for 1 h at 20 $^{\circ}\text{C}$ prior to addition of 10 mM NaCl and subsequent centrifugation for 2 h at 4 $^{\circ}\text{C}$. Dashed lines represent fitted components.

Panel A represents the control situation: the fully active enzyme is in 20 mM histidine (His) and all preparation procedures, including centrifugation, were performed at 4 °C. **Figure 19A** shows the first heating scan; for this and all other samples, the thermal denaturation is irreversible. Neither the cooling nor the reheating scans contained any transition peaks, and the post-transitional baselines at the end of the first heating scans showed no signs of sample aggregation. The thermal unfolding is not a simple single two-state transition; up to four components are required to fit the complete endotherm. Heats of unfolding and mid-point temperatures of the component peaks are listed in **Table 4**. The peak maximum of the overall endotherm is at 45 °C, but components with comparable heats of unfolding are present at 33, 41 and 50 °C.

Condition	Activity (%)	T_m (°C)	T_d (°C)	ΔH_d (kcal·mol ⁻¹)	ΔH_{tot} (kcal·mol ⁻¹)
20 mM His no preincubation	110 ± 5	44.5	33.2	80	437
			41.5	115	
			45.1	139	
			50.2	103	
20 mM His preincubated 1 h at 20 °C	108 ± 6	45.2	36.5	95	511
			43.0	133	
			46.1	153	
			51.1	130	
1 mM His no preincubation	64 ± 8	36.4	32.8	90	282
			37.5	106	
			48.2	86	
1 mM His preincubated 1 h at 20 °C, 10 mM NaCl added before centrifugation	27 ± 4	50.7	42.7	65	313
			47.2	120	
			52.3	128	

Table 4: Mid-point temperatures, T_d , and heats of transition, ΔH_d , of the components fitting the calorimetric endotherms of membranous shark Na,K-ATPase. ΔH_{tot} and T_m are the heat of transition mid-point temperature of the entire endotherm. The ATPase activity is expressed as percentage of that of the native enzyme without incubation or centrifugation.

Figure 19B shows the first heating scan for shark enzyme in 20 mM histidine that was preincubated for 1 h at 20 °C prior to centrifugation at 4 °C. The shape of the endotherm is

similar to that of the sample that was not preincubated at 20 °C, and the total enthalpy is similar to that of the control (see **Table 4**). This result correlates with the protection of the shark enzyme against inactivation that is afforded by 20 mM histidine. **Figure 19C** shows the first DSC heating scan for shark enzyme in 1 mM histidine that was kept at 4 °C during the sample preparation and not preincubated at higher temperature prior to centrifugation. The result is a considerable change in shape of the endotherm and reduction in overall heat of transition (see **Table 4**), relative to control enzyme in 20 mM histidine. In principal, heat is lost from components of the control endotherm that occur at higher temperature (**Figure 19A**). This reduction in heat of unfolding correlates with the inactivation of the shark enzyme by centrifugation at low ionic strength and also with the steady rate of inactivation on incubation in 1 mM histidine at 4 °C. Addition of 10 mM NaCl protects against inactivation during centrifugation. **Figure 19D** shows the first DSC heating scan of shark enzyme in 1 mM histidine that was preincubated for 1 h at 20 °C, but to which 10 mM NaCl was then added prior to centrifugation at 4 °C (NaCl was present during the centrifugation step only). Again, the shape of the calorimetric endotherm differs considerably from that of the control (**Figure 19A**), but in a very different way from that of the enzyme in 1 mM histidine that was not preincubated but lacked NaCl in the centrifugation step (**Figure 19C**). In this case (**Figure 19D**), heat is lost from the components occurring at lower temperature in the control sample. This corresponds to the ~70% inactivation of the shark enzyme, which is accounted for completely by the incubation at 20 °C or 1 h in 1 mM histidine in the absence of NaCl. Addition of 10 mM NaCl protects against inactivation during centrifugation, where the latter corresponds to the loss of transition heat from the higher temperature components of the endotherm that is found in **Figure 19C**.

4.5. Differential scanning calorimetry of pig kidney Na,K-ATPase containing membranes

The DSC heating scans for membranous Na,K-ATPase preparations from pig kidney are shown in **Figure 20** under the various conditions used for the shark enzyme in **Figure 19**.

The thermal unfolding of the pig kidney enzyme takes place at a higher temperature than that for the shark enzyme. The heat capacity maximum occurs at 54 °C for the control

sample in 20 mM histidine (**Figure 20A**). The shape of the denaturation endotherm of the pig kidney Na,K-ATPase also differs from that for the shark enzyme. It similarly consists of several components, but is distinguished from the endotherm of the shark enzyme by broad transitions lying at higher temperature.

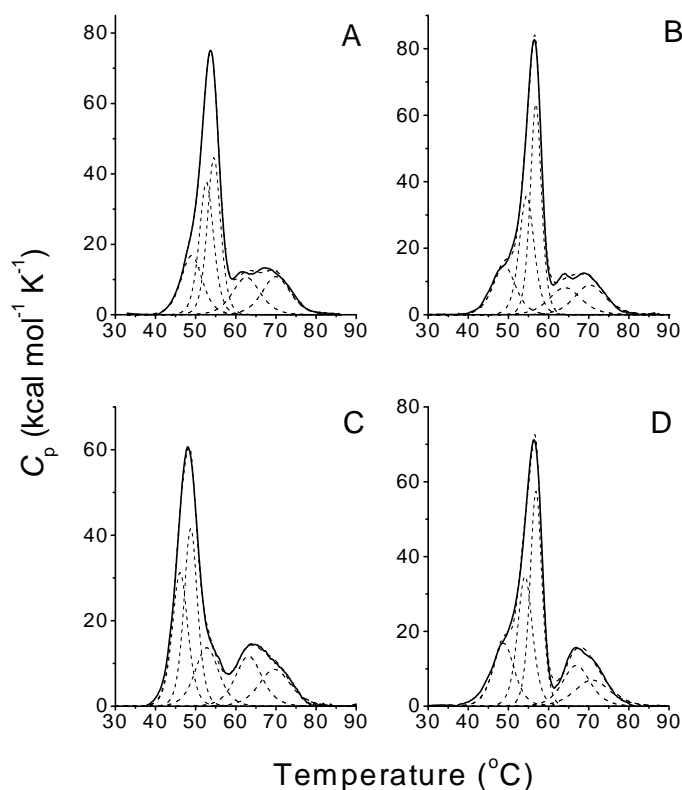


Figure 20: Excess heat capacity functions of membranous Na,K-ATPase from pig kidney, after baseline subtraction. (A) Enzyme in 20 mM histidine, centrifuged for 2 h at 4 °C. (B) Enzyme in 20 mM histidine, preincubated for 1 h at 20 °C prior to centrifugation for 2 h at 4 °C. (C) Enzyme in 1 mM histidine, centrifuged for 2 h at 4 °C. (D) Enzyme in 1mM histidine, preincubated for 1 h at 20 °C prior to addition of 10 mM NaCl and subsequent centrifugation for 2 h at 4 °C. Dashed lines represent fitted components.

Mid-point temperatures and corresponding heats of transition for the different components are listed in **Table 5**.

Condition	Activity (%)	T_m (°C)	T_d (°C)	ΔH_d (kcal·mol ⁻¹)	ΔH_{tot} (kcal·mol ⁻¹)
20 mM His no preincubation	87 ± 9	53.7	49.0	118	690
			52.7	178	
			54.6	195	
			62.7	98	
			70.1	101	
20 mM His preincubated 1 h at 20 °C	82 ± 5	56.5	49	110	696
			54.6	175	
			56.8	234	
			64.2	86	
			70.3	92	
1 mM His no preincubation	84 ± 6	47.9	46.1	160	643
			48.8	185	
			52.8	107	
			63.2	102	
			69.7	90	
1 mM His preincubated 1 h at 20 °C, 10 mM NaCl added before centrifugation	86 ± 9	56.4	48.8	118	694
			54.2	172	
			56.9	223	
			67.0	100	

Table 5: Mid-point temperatures, T_d , and heats of transition, ΔH_d , of the components fitting the calorimetric endotherms of membranous pig kidney Na,K-ATPase. ΔH_{tot} and T_m are the heat of transition mid-point temperature of the entire endotherm. The ATPase activity is expressed as percentage of that of the native enzyme without incubation or centrifugation.

Also, unlike the shark enzyme, the thermal unfolding of the pig kidney enzyme does not depend greatly on the ionic and incubation conditions. In particular, the total heat of unfolding remains the same for all four endotherms in **Figure 20** (see **Table 5**). Centrifugation of the pig enzyme in 1 mM histidine did, however, shift the overall endotherm to lower temperature (compare **Figure 20A** and **C**).

Despite the identity of the general architecture and close similarity of their primary structures, Na,K-ATPase enzymes isolated from shark salt gland and pig kidney preparations demonstrate differences in their thermal stability and denaturation temperatures. The pig enzyme is much more stable towards thermal denaturation than the shark enzyme,

and this structural stability is correlated with previous enzymatic stability measurements [93]. The present thermal denaturation studies demonstrated incomplete unfolding of Na,K-ATPase. The multiple components in the overall unfolding transition could be attributed either to different steps in the unfolding pathway or to independent unfolding of different domains (or to a combination of both). The removal of different specific components by centrifugation or by incubation at elevated temperature at low ionic strength favours an interpretation in terms of domain unfolding, at least for the shark enzyme. Because the high thermodynamic stability of H-bonding in the hydrophobic environment of the TM helices, it is expected that the principal unfolding transitions are confined largely to the extramembranous sections of the protein. The adaptation of the thermal stability of the sections of the protein in contact mainly with water is a very surprising observation because evolution has no way to change the temperature dependence of the dynamics of water, as opposed to that of the biomembrane.

Summary

Main results on the yeast vacuolar H⁺-ATPase

1. We standardised the conditions (temperature, reaction time, substrate concentration, selective inhibitor) in native vacuolar membrane for steady state activity measurement and determined that 60% of the total ATPase activity attributable to V-ATPase.

2. We developed a method to measure V-ATPase activity in the absence and presence of an externally applied alternating (AC) electric field in the native vacuolar vesicles.

3. We performed the first of its kind of experiment by applying an oscillating electric field on the V-ATPase which allowed us to measure the rate of rotation in native V-ATPase.

4. A resonant like effect was detected between 87 Hz and 94 Hz and was shown that, according to the two-channel model, it corresponds to the 60° step of the rotor. The so obtained rate of rotation of ~14 Hz agrees very well with the low limit estimate of ~10 Hz from steady state activity and inhibitor titration experiment.

5. We demonstrated that the AC field effect acts via a transmembrane potential, because by adding ionophores to the membrane suspension, the effect diminished.

To our knowledge, these are the first data of the rotation rate of yeast V-ATPase in its native membrane environment.

Main results on the stability of Na,K-ATPase

1. The thermal unfolding curves of both types of Na,K-ATPase show the presence of multiple components, which can be attributed to different steps in the unfolding pathway or to independent unfolding of different domains.

2. We have shown that the pig enzyme is much more stable towards thermal denaturation as compared with the shark enzyme, since its heat capacity maxima occur at 54 °C and 48 °C versus 45 °C and 36 °C for the shark enzyme in the presence of 20 mM and 1 mM histidine, respectively.

3. We measured almost the same degree of stabilisation effect for both enzymes when preincubated at 20 °C with 20 mM histidine proving that high concentration of histidine is capable of stabilising these enzymes.

4. We have shown that increasing ionic strength increases the stability of both enzymes: adding 10 mM NaCl to the pig and the shark enzyme, both preincubated with 1 mM histidine at 20 °C shifted their heat capacity maxima from 48 °C to 56 °C, and from 36 °C to 50 °C, respectively.

References

1. Farina, C. and Gagliardi, S.: **Selective inhibitors of the osteoclast vacuolar proton ATPase as novel bone antiresorptive agents**, *Drug discovery today* 1999, **4**: 163-172
2. Bowman, E.J. and Bowman, B.J.: **V-ATPases as drug targets**, *Journal of bioenergetics and biomembranes* 2005, **37**: 431-435
3. Lu, X., Qin, W., Li, J., Tan, N., Pan, D., Zhang, H., Xie, L., Yao, G., Shu, H., Yao, M., Wan, D., Gu, J. and Yang, S.: **The growth and metastasis of human hepatocellular carcinoma xenografts are inhibited by small interfering RNA targeting to the subunit ATP6L of proton pump**, *Cancer research* 2005, **65**: 6843-6849
4. Morimura, T., Fujita, K., Akita, M., Nagashima, M. and Satomi, A.: **The proton pump inhibitor inhibits cell growth and induces apoptosis in human hepatoblastoma**, *Pediatric surgery international* 2008, **24**: 1087-1094
5. McHenry, P., Wang, W.W., Devitt, E., Kluesner, N., Davisson, V.J., McKee, E., Schweitzer, D., Helquist, P. and Tenniswood, M.: **Iejimalides A and B inhibit lysosomal vacuolar H⁺-ATPase (V-ATPase) activity and induce S-phase arrest and apoptosis in MCF-7 cells**, *Journal of cellular biochemistry* 2010, **109**: 634-642
6. Yoshida, M., Muneyuki, E. and Hisabori, T.: **ATP synthase-a marvellous rotary engine of the cell**, *Nature reviews. Molecular cell biology* 2001, **2**: 669-677
7. Imamura, H., Nakano, M., Noji, H., Muneyuki, E., Ohkuma, S., Yoshida, M. and Yokoyama, K.: **Evidence for rotation of V1-ATPase**, *Proceedings of the National Academy of Sciences of the United States of America* 2003, **100**: 2312-2315
8. Nishi, T. and Forgac, M.: **The vacuolar (H⁺)-ATPases--nature's most versatile proton pumps**, *Nature reviews. Molecular cell biology* 2002, **3**: 94-103
9. Domgall, I., Venzke, D., Lüttge, U., Ratajczak, R. and Böttcher, B.: **Three-dimensional map of a plant V-ATPase based on electron microscopy**, *The Journal of biological chemistry* 2002, **277**: 13115-13121
10. Wilkens, S., Vasilyeva, E. and Forgac, M.: **Structure of the vacuolar ATPase by electron microscopy**, *The Journal of biological chemistry* 1999, **274**: 31804-31810
11. Boekema, E.J., van Breemen, J.F., Brisson, A., Ubbink-Kok, T., Konings, W.N. and Lolkema, J.S.: **Connecting stalks in V-type ATPase**, *Nature* 1999, **401**: 37-38
12. Noji, H., Yasuda, R., Yoshida, M. and Kinosita, K.J.: **Direct observation of the rotation of F1-ATPase**, *Nature* 1997, **386**: 299-302

13. Nelson, N., Sacher, A. and Nelson, H.: **The significance of molecular slips in transport systems**, *Nature reviews. Molecular cell biology* 2002, **3**: 876-881
14. Noumi, T., Beltrán, C., Nelson, H. and Nelson, N.: **Mutational analysis of yeast vacuolar H(+)-ATPase**, *Proceedings of the National Academy of Sciences of the United States of America* 1991, **88**: 1938-1942
15. Hirata, R., Graham, L.A., Takatsuki, A., Stevens, T.H. and Anraku, Y.: **VMA11 and VMA16 encode second and third proteolipid subunits of the *Saccharomyces cerevisiae* vacuolar membrane H⁺-ATPase**, *The Journal of biological chemistry* 1997, **272**: 4795-4803
16. Yasuda, R., Noji, H., Kinosita, K.J., Motojima, F. and Yoshida, M.: **Rotation of the gamma subunit in F1-ATPase; evidence that ATP synthase is a rotary motor enzyme**, *Journal of bioenergetics and biomembranes* 1997, **29**: 207-209
17. Yasuda, R., Noji, H., Yoshida, M., Kinosita, K.J. and Itoh, H.: **Resolution of distinct rotational substeps by submillisecond kinetic analysis of F1-ATPase**, *Nature* 2001, **410**: 898-904
18. Fillingame, R.H., Jiang, W. and Dmitriev, O.Y.: **Coupling H(+) transport to rotary catalysis in F-type ATP synthases: structure and organization of the transmembrane rotary motor**, *The Journal of experimental biology* 2000, **203**: 9-17
19. Ueno, H., Suzuki, T., Kinosita, K.J. and Yoshida, M.: **ATP-driven stepwise rotation of FoF1-ATP synthase**, *Proceedings of the National Academy of Sciences of the United States of America* 2005, **102**: 1333-1338
20. Futai, M., Omote, H., Sambongi, Y. and Wada, Y.: **Synthase (H(+) ATPase): coupling between catalysis, mechanical work, and proton translocation**, *Biochimica et biophysica acta* 2000, **1458**: 276-288
21. Ubbink-Kok, T., Boekema, E.J., van Breemen, J.F., Brisson, A., Konings, W.N. and Lolkema, J.S.: **Stator structure and subunit composition of the V(1)/V(0) Na(+)-ATPase of the thermophilic bacterium *Caloramator fervidus***, *Journal of molecular biology* 2000, **296**: 311-321
22. Boekema, E.J., Ubbink-Kok, T., Lolkema, J.S., Brisson, A. and Konings, W.N.: **Visualization of a peripheral stalk in V-type ATPase: evidence for the stator structure essential to rotational catalysis**, *Proceedings of the National Academy of Sciences of the United States of America* 1997, **94**: 14291-14293
23. Ohira, M., Smardon, A.M., Charsky, C.M.H., Liu, J., Tarsio, M. and Kane, P.M.: **The E and G subunits of the yeast V-ATPase interact tightly and are both present at more than one copy per V1 complex**, *The Journal of biological chemistry* 2006, **281**: 22752-22760

24. Sambade, M. and Kane, P.M.: **The yeast vacuolar proton-translocating ATPase contains a subunit homologous to the *Manduca sexta* and bovine e subunits that is essential for function**, *The Journal of biological chemistry* 2004, **279**: 17361-17365
25. Powell, B., Graham, L.A. and Stevens, T.H.: **Molecular characterization of the yeast vacuolar H⁺-ATPase proton pore**, *The Journal of biological chemistry* 2000, **275**: 23654-23660
26. Gibson, L.C.D., Cadwallader, G. and Finbow, M.E.: **Evidence that there are two copies of subunit c" in V0 complexes in the vacuolar H⁺-ATPase**, *The Biochemical journal* 2002, **366**: 911-919
27. Holzenburg, A., Jones, P.C., Franklin, T., Pali, T., Heimburg, T., Marsh, D., Findlay, J.B. and Finbow, M.E.: **Evidence for a common structure for a class of membrane channels**, *European journal of biochemistry / FEBS* 1993, **213**: 21-30
28. El Far, O. and Seagar, M.: **A role for V-ATPase subunits in synaptic vesicle fusion?**, *Journal of neurochemistry* 2011, **117**: 603-612
29. Baars, T.L., Petri, S., Peters, C. and Mayer, A.: **Role of the V-ATPase in regulation of the vacuolar fission-fusion equilibrium**, *Molecular biology of the cell* 2007, **18**: 3873-3882
30. Strasser, B., Iwaszkiewicz, J., Michielin, O. and Mayer, A.: **The V-ATPase proteolipid cylinder promotes the lipid-mixing stage of SNARE-dependent fusion of yeast vacuoles**, *The EMBO journal* 2011, **30**: 4126-4141
31. Kawasaki-Nishi, S., Nishi, T. and Forgac, M.: **Arg-735 of the 100-kDa subunit a of the yeast V-ATPase is essential for proton translocation**, *Proceedings of the National Academy of Sciences of the United States of America* 2001, **98**: 12397-12402
32. Manolson, M.F., Wu, B., Proteau, D., Taillon, B.E., Roberts, B.T., Hoyt, M.A. and Jones, E.W.: **STV1 gene encodes functional homologue of 95-kDa yeast vacuolar H⁽⁺⁾-ATPase subunit Vph1p**, *The Journal of biological chemistry* 1994, **269**: 14064-14074
33. Iwata, M., Imamura, H., Stambouli, E., Ikeda, C., Tamakoshi, M., Nagata, K., Makyio, H., Hankamer, B., Barber, J., Yoshida, M., Yokoyama, K. and Iwata, S.: **Crystal structure of a central stalk subunit C and reversible association/dissociation of vacuole-type ATPase**, *Proceedings of the National Academy of Sciences of the United States of America* 2004, **101**: 59-64
34. Ludwig, J., Kerscher, S., Brandt, U., Pfeiffer, K., Getlawi, F., Apps, D.K. and Schägger, H.: **Identification and characterization of a novel 9.2-kDa membrane sector-associated protein of vacuolar proton-ATPase from chromaffin granules**, *The Journal of biological chemistry* 1998, **273**: 10939-10947

35. Merzendorfer, H., Huss, M., Schmid, R., Harvey, W.R. and Wieczorek, H.: **A novel insect V-ATPase subunit M9.7 is glycosylated extensively**, *The Journal of biological chemistry* 1999, **274**: 17372-17378
36. Boyer, P.D. and Kohlbrenner, W.E.: **The present status of the binding-change mechanism and its relation to ATP formation by chloroplasts**. In *Energy coupling in photosynthesis*, eds. Selman, B.R. and Selman-Reiner, S. (Elsevier, Amsterdam), 1981, pp. 231-240
37. Boyer, P.D.: **The binding change mechanism for ATP synthase-some probabilities and possibilities**, *Biochimica et biophysica acta* 1993, **1140**: 215-250
38. Shimabukuro, K., Yasuda, R., Muneyuki, E., Hara, K.Y., Kinosita, K.J. and Yoshida, M.: **Catalysis and rotation of F1 motor: cleavage of ATP at the catalytic site occurs in 1 ms before 40 degree substep rotation**, *Proceedings of the National Academy of Sciences of the United States of America* 2003, **100**: 14731-14736
39. Yasuda, R., Noji, H., Kinosita, K.J. and Yoshida, M.: **F1-ATPase is a highly efficient molecular motor that rotates with discrete 120 degree steps**, *Cell* 1998, **93**: 1117-1124
40. Vik, S.B., Long, J.C., Wada, T. and Zhang, D.: **A model for the structure of subunit a of the Escherichia coli ATP synthase and its role in proton translocation**, *Biochimica et biophysica acta* 2000, **1458**: 457-466
41. Fillingame, R.H., Angevine, C.M. and Dmitriev, O.Y.: **Coupling proton movements to c-ring rotation in F(1)F(o) ATP synthase: aqueous access channels and helix rotations at the a-c interface**, *Biochimica et biophysica acta* 2002, **1555**: 29-36
42. Junge, W., Pänke, O., Cherepanov, D.A., Gumbiowski, K., Müller, M. and Engelbrecht, S.: **Inter-subunit rotation and elastic power transmission in F0F1-ATPase**, *FEBS letters* 2001, **504**: 152-160
43. Forgac, M.: **Vacuolar ATPases: rotary proton pumps in physiology and pathophysiology**, *Nature reviews. Molecular cell biology* 2007, **8**: 917-929
44. Kawasaki-Nishi, S., Nishi, T. and Forgac, M.: **Interacting helical surfaces of the transmembrane segments of subunits a and c' of the yeast V-ATPase defined by disulfide-mediated cross-linking**, *The Journal of biological chemistry* 2003, **278**: 41908-41913
45. Wang, Y., Inoue, T. and Forgac, M.: **TM2 but not TM4 of subunit c'' interacts with TM7 of subunit a of the yeast V-ATPase as defined by disulfide-mediated cross-linking**, *The Journal of biological chemistry* 2004, **279**: 44628-44638

46. Yokoyama, K., Nakano, M., Imamura, H., Yoshida, M. and Tamakoshi, M.: **Rotation of the proteolipid ring in the V-ATPase**, *The Journal of biological chemistry* 2003, **278**: 24255-24258
47. Hirata, T., Iwamoto-Kihara, A., Sun-Wada, G., Okajima, T., Wada, Y. and Futai, M.: **Subunit rotation of vacuolar-type proton pumping ATPase: relative rotation of the G and C subunits**, *The Journal of biological chemistry* 2003, **278**: 23714-23719
48. Aviezer-Hagai, K., Padler-Karavani, V. and Nelson, N.: **Biochemical support for the V-ATPase rotary mechanism: antibody against HA-tagged Vma7p or Vma16p but not Vma10p inhibits activity**, *The Journal of experimental biology* 2003, **206**: 3227-3237
49. Imamura, H., Ikeda, C., Yoshida, M. and Yokoyama, K.: **The F subunit of Thermus thermophilus V1-ATPase promotes ATPase activity but is not necessary for rotation**, *The Journal of biological chemistry* 2004, **279**: 18085-18090
50. Imamura, H., Takeda, M., Funamoto, S., Shimabukuro, K., Yoshida, M. and Yokoyama, K.: **Rotation scheme of V1-motor is different from that of F1-motor**, *Proceedings of the National Academy of Sciences of the United States of America* 2005, **102**: 17929-17933
51. Furuike, S., Nakano, M., Adachi, K., Noji, H., Kinoshita, K.J. and Yokoyama, K.: **Resolving stepping rotation in Thermus thermophilus H(+)-ATPase/synthase with an essentially drag-free probe**, *Nature Communication* 2011, **2**: 233
52. Masaike, T., Mitome, N., Noji, H., Muneyuki, E., Yasuda, R., Kinoshita, K. and Yoshida, M.: **Rotation of F(1)-ATPase and the hinge residues of the beta subunit**, *The Journal of experimental biology* 2000, **203**: 1-8
53. Itoh, H., Takahashi, A., Adachi, K., Noji, H., Yasuda, R., Yoshida, M. and Kinoshita, K.: **Mechanically driven ATP synthesis by F1-ATPase**, *Nature* 2004, **427**: 465-468
54. Adachi, K., Oiwa, K., Nishizaka, T., Furuike, S., Noji, H., Itoh, H., Yoshida, M. and Kinoshita, K.J.: **Coupling of rotation and catalysis in F(1)-ATPase revealed by single-molecule imaging and manipulation**, *Cell* 2007, **130**: 309-321
55. Takeda, M., Suno-Ikeda, C., Shimabukuro, K., Yoshida, M. and Yokoyama, K.: **Mechanism of inhibition of the V-type molecular motor by tributyltin chloride**, *Biophysical journal* 2009, **96**: 1210-1217
56. Lutsenko, S. and Kaplan, J.H.: **Organization of P-type ATPases: significance of structural diversity**, *Biochemistry* 1995, **34**: 15607-15613
57. Sachs, G. and Munson, K.: **Mammalian phosphorylating ion-motive ATPases**, *Current opinion in cell biology* 1991, **3**: 685-694

58. Repke, K.R. and Schön, R.: **Role of protein conformation changes and transphosphorylations in the function of Na⁺/K⁺-transporting adenosine triphosphatase: an attempt at an integration into the Na⁺/K⁺ pump mechanism**, *Biological reviews of the Cambridge Philosophical Society* 1992, **67**: 31-78
59. Skou, J.C. and Esmann, M.: **The Na,K-ATPase**, *Journal of bioenergetics and biomembranes* 1992, **24**: 249-261
60. Teriete, P., Franzin, C.M., Choi, J. and Marassi, F.M.: **Structure of the Na,K-ATPase regulatory protein FXYD1 in micelles**, *Biochemistry* 2007, **46**: 6774-6783
61. Geering, K.: **Functional roles of Na,K-ATPase subunits**, *Current opinion in nephrology and hypertension* 2008, **17**: 526-532
62. Blanco, G. and Mercer, R.W.: **Isozymes of the Na-K-ATPase: heterogeneity in structure, diversity in function**, *The American journal of physiology* 1998, **275**: F633-50
63. Albers, R.W.: **Biochemical aspects of active transport**, *Annual review of biochemistry* 1967, **36**: 727-756
64. Post, R.L., Hegyvary, C. and Kume, S.: **Activation by adenosine triphosphate in the phosphorylation kinetics of sodium and potassium ion transport adenosine triphosphatase**, *The Journal of biological chemistry* 1972, **247**: 6530-6540
65. Horisberger, J.D., Lemas, V., Kraehenbühl, J.P. and Rossier, B.C.: **Structure-function relationship of Na,K-ATPase**, *Annual review of physiology* 1991, **53**: 565-584
66. Horisberger, J.: **Recent insights into the structure and mechanism of the sodium pump**, *Physiology (Bethesda, Md.)* 2004, **19**: 377-387
67. Gadsby, D.C., Takeuchi, A., Artigas, P. and Reyes, N.: **Review. Peering into an ATPase ion pump with single-channel recordings**, *Philosophical transactions of the Royal Society of London. Series B, Biological sciences* 2009, **364**: 229-238
68. Lew, V.L., Glynn, I.M. and Ellory, J.C.: **Net synthesis of ATP by reversal of the sodium pump**, *Nature* 1970, **225**: 865-866
69. Kaplan, J.H.: **Biochemistry of Na,K-ATPase**, *Annual review of biochemistry* 2002, **71**: 511-535
70. Møller, J.V., Juul, B. and le Maire, M.: **Structural organization, ion transport, and energy transduction of P-type ATPases**, *Biochimica et biophysica acta* 1996, **1286**: 1-51

71. Uchida, E., Ohsumi, Y. and Anraku, Y.: **Purification and properties of H⁺-translocating, Mg²⁺-adenosine triphosphatase from vacuolar membranes of *Saccharomyces cerevisiae***, *The Journal of biological chemistry* 1985, **260**: 1090-1095
72. Ohsumi, Y. and Anraku, Y.: **Active transport of basic amino acids driven by a proton motive force in vacuolar membrane vesicles of *Saccharomyces cerevisiae***, *The Journal of biological chemistry* 1981, **256**: 2079-2082
73. Lowry, O.H., Rosebrough, N.J., Farr, A.L. and Randall, R.J.: **Protein measurement with the Folin phenol reagent**, *The Journal of biological chemistry* 1951, **193**: 265-275
74. Severs, N.J.: **Freeze-fracture electron microscopy**, *Nature protocols* 2007, **2**: 547-576
75. Clelland, E.S. and Saleuddin, A.S.: **Vacuolar-type ATPase in the accessory boring organ of *Nucella lamellosa* (Gmelin) (Mollusca : Gastropoda): role in shell penetration**, *The Biological bulletin* 2000, **198**: 272-283
76. Serrano, R.: **Characterization of the plasma membrane ATPase of *Saccharomyces cerevisiae***, *Molecular and cellular biochemistry* 1978, **22**: 51-63
77. Padilla-López, S. and Pearce, D.A.: ***Saccharomyces cerevisiae* lacking Btn1p modulate vacuolar ATPase activity to regulate pH imbalance in the vacuole**, *The Journal of biological chemistry* 2006, **281**: 10273-10280
78. Lunde, C.S. and Kubo, I.: **Effect of polygodial on the mitochondrial ATPase of *Saccharomyces cerevisiae***, *Antimicrobial agents and chemotherapy* 2000, **44**: 1943-1953
79. Zrimec, A., Jerman, I. and Lahajnar, G.: **Low frequency alternating electric fields inhibit lactose uptake in *Kluyveromyces marxianus***, *Bioelectrochemistry and bioenergetics (Lausanne, Switzerland)* 1999, **48**: 481-484
80. Zrimec, A., Jerman, I. and Lahajnar, G.: **Alternating electric fields stimulate ATP synthesis in *Escherichia coli***, *Cellular and molecular biology letters* 2002, **7**: 172-174
81. Skou, J.C. and Esmann, M.: **Preparation of membrane-bound and of solubilized (Na⁺ + K⁺)-ATPase from rectal glands of *Squalus acanthias*. The effect of preparative procedures on purity, specific and molar activity**, *Biochimica et biophysica acta* 1979, **567**: 436-444
82. Jorgensen, P.L.: **Purification and characterization of (Na⁺ plus K⁺)-ATPase. 3. Purification from the outer medulla of mammalian kidney after selective removal of membrane components by sodium dodecylsulphate**, *Biochimica et biophysica acta* 1974, **356**: 36-52

83. Klodos, I., Esmann, M. and Post, R.L.: **Large-scale preparation of sodium-potassium ATPase from kidney outer medulla**, *Kidney international* 2002, **62**: 2097-2100
84. Esmann, M.: **ATPase and phosphatase activity of Na⁺,K⁺-ATPase: molar and specific activity, protein determination**, *Methods in enzymology* 1988, **156**: 105-115
85. Páli, T., Whyteside, G., Dixon, N., Kee, T.P., Ball, S., Harrison, M.A., Findlay, J.B.C., Finbow, M.E. and Marsh, D.: **Interaction of inhibitors of the vacuolar H⁽⁺⁾-ATPase with the transmembrane Vo-sector**, *Biochemistry* 2004, **43**: 12297-12305
86. Huss, M., Ingenhorst, G., König, S., Gassel, M., Dröse, S., Zeeck, A., Altendorf, K. and Wiczorek, H.: **Concanamycin A, the specific inhibitor of V-ATPases, binds to the V(o) subunit c**, *The Journal of biological chemistry* 2002, **277**: 40544-40548
87. Kóta, Z., Páli, T., Dixon, N., Kee, T.P., Harrison, M.A., Findlay, J.B.C., Finbow, M.E. and Marsh, D.: **Incorporation of transmembrane peptides from the vacuolar H⁽⁺⁾-ATPase in phospholipid membranes: spin-label electron paramagnetic resonance and polarized infrared spectroscopy**, *Biochemistry* 2008, **47**: 3937-3949
88. Beyenbach, K.W. and Wiczorek, H.: **The V-type H⁺ ATPase: molecular structure and function, physiological roles and regulation**, *The Journal of experimental biology* 2006, **209**: 577-589
89. Junge, W., Lill, H. and Engelbrecht, S.: **ATP synthase: an electrochemical transducer with rotatory mechanics**, *Trends in biochemical sciences* 1997, **22**: 420-423
90. Feniouk, B.A., Kozlova, M.A., Knorre, D.A., Cherepanov, D.A., Mulkidjanian, A.Y. and Junge, W.: **The proton-driven rotor of ATP synthase: ohmic conductance (10 fS), and absence of voltage gating**, *Biophysical journal* 2004, **86**: 4094-4109
91. Grabe, M., Wang, H. and Oster, G.: **The mechanochemistry of V-ATPase proton pumps**, *Biophysical journal* 2000, **78**: 2798-2813
92. Murata, T., Yamato, I., Kakinuma, Y., Leslie, A.G.W. and Walker, J.E.: **Structure of the rotor of the V-Type Na⁺-ATPase from *Enterococcus hirae***, *Science* 2005, **308**: 654-659
93. Fodor, E., Fedosova, N.U., Ferencz, C., Marsh, D., Pali, T. and Esmann, M.: **Stabilization of Na,K-ATPase by ionic interactions**, *Biochimica et biophysica acta* 2008, **1778**: 835-843